Supramolecular Chemistry
Publication details, including instructions for authors and subscription information:
http://www.informaworld.com/smpp/title~content=t713649759

Evaluating the Conformational Role of an Allosteric Cu^{II} Ion in Anion Recognition and Catalysis by a Tricopper Complex

Kai P. Strotmeyer[a]; Igor O. Fritsky[b]; Reina Ott[a]; Hans Pritzkow[a]; Roland Krämer[a]
[a] Anorganisch-Chemisches Institut der Universität Heidelberg, Heidelberg, Germany [b] Department of Chemistry, Shevchenko University, Kiev, Ukraine

Online publication date: 13 May 2010

To cite this Article Strotmeyer, Kai P. , Fritsky, Igor O. , Ott, Reina , Pritzkow, Hans and Krämer, Roland(2003) 'Evaluating the Conformational Role of an Allosteric Cu^{II} Ion in Anion Recognition and Catalysis by a Tricopper Complex', Supramolecular Chemistry, 15: 7, 529 — 547
To link to this Article: DOI: 10.1080/1061027031000160124
URL: http://dx.doi.org/10.1080/10610270310001605124

Supramolecular Chemistry, 2003 Vol. 15 (7–8), pp. 529–547

Evaluating the Conformational Role of an Allosteric Cu^{II} Ion in Anion Recognition and Catalysis by a Tricopper Complex

KAI P. STROTMEYER[a], IGOR O. FRITSKY[b], REINA OTT[a], HANS PRITZKOW[a] and ROLAND KRÄMER[a,*]

[a]*Anorganisch-Chemisches Institut der Universität Heidelberg, Im Neuenheimer Feld 270, D-69120 Heidelberg, Germany;* [b]*Department of Chemistry, Shevchenko University, Kiev 01033, Ukraine*

Received 4 November 2002; Accepted 17 December 2002

Structural and anion binding studies have provided an insight into the conformational role of an allosteric Cu^{II} ion in the trinuclear catalyst $(L^2–2H)Cu_3^{II}$. L^2 is a novel trinucleating ligand with pyridyl, pyrimidyl and amide donor groups. $(L^2–2H)Cu$ (1) has been characterized by X-ray crystallography. The Cu ion is located at the allosteric site and coordinated by two amide N and two pyrimidine N atoms, the CuN_4 plane is tetrahedrally distorted, and the complex adopts a helically twisted conformation. In contrast, the $(L^2–2H)Cu_3(\mu_4\text{-}C_2O_4)$ subunit of the dodecanuclear complex $[(L^2–2H)_4Cu_{12}(\mu_4\text{-}C_2O_4)_2(\mu\text{-}OH)_4(\mu\text{-}Cl)_4\text{-}Cl_4(H_2O)_2]$ (5) is roof-shaped, and the allosteric Cu is located on the top of a square-based pyramid. The oxalate coligand is coordinated by the two catalytic Cu ions in an unusual 1,4-μ-O,O bridging mode with an O···O "bite length" of 2.6 Å and a Cu···Cu distance of 6.4 Å. Intramolecular transesterification of the phosphodiester 2-(hydroxypropyl)-*p*-nitrophenyl phosphate (HPNP) by $[(L^2–2H)Cu_3]^{4+}$ was investigated, in comparison with the closely related complex $[(L^3–2H)Cu_3]^{4+}$ in which the ligand framework is somewhat less flexible. From a kinetic analysis of cleavage rate at varying HPNP concentrations, K_{HPNP} (the equilibrium constant for binding of HPNP to the complex) and k_{cat} (first-order rate constant for cleavage of HPNP when bound to the complex) parameters were derived: $K_{HPNP} = 190\ M^{-1}$ ($[(L^2–2H)Cu_3]^{4+}$) and $305\ M^{-1}$ ($[(L^3–2H)Cu_3]^{4+}$), $k_{cat} = 10 \times 10^{-3}\ s^{-1}$ ($[(L^2–2H)Cu_3]^{4+}$) and $3.3 \times 10^{-3}\ s^{-1}$ ($[(L^3–2H)Cu_3]^{4+}$). Anion binding constants of the complexes were determined by monitoring competitive inhibition of HPNP cleavage. The complexes

The Future of Supramolecular Chemistry

Self-assembly involving coordination chemistry has recently undergone a particularly tremendous development, making available many fascinating complex structures by relatively simple and rapid synthetic procedures. Much has been learned about the use of directional bonding afforded by metal centres for the rational assembly of supramolecular architectures. In view of recent breakthroughs in the engineering of prototypical molecular scale electronic circuits, it is a very exciting challenge to create nanosized structures by self-assembly and to individually control their physical properties for "bottom up" solutions of problems to miniaturisation.

Roland Krämer (born 1963) undertook undergraduate studies at the universities of Karlsruhe and Munich. He received his PhD in Munich 1991 in Professor W. Beck's laboratory (organometallic chemistry) and was a postdoc 1991–1992 in the lab of J.-M. Lehn at Strasbourg (inorganic self-assembly). In 1997, he finished his Habilitation at University of Münster (bioinorganic Chemistry) and became a professor at the University of Heidelberg in 1999. His research interests include coordination, bioinorganic and bioconjugate chemistry.

*Corresponding author. Fax: +49-6221-548439. E-mail: roland.kraemer@urz.uni-heidelberg.de

ISSN 1061-0278 print/ISSN 1029-0478 online © 2003 Taylor & Francis Ltd
DOI: 10.1080/1061027031000160512 4

have a high affinity to SO_4^{2-}, HPO_4^{2-}, and ReO_4^-, which appear to be of the appropriate size for bridging coordination, while "smaller" anions $CH_3CO_2^-$ and HCO_3^- are bound less efficiently. $[(L^3{-}2H)Cu_3]^{4+}$ has a higher affinity than $[(L^2{-}2H)Cu_3]^{4+}$ to HPNP but a lower affinity to the rather large anion ReO_4^-. This is interpreted as a consequence of the reduced flexibility of $[(L^3{-}2H)Cu_3]^{4+}$, which slightly disfavours widening of the Cu···Cu distance for incorporation of perrhenate. Similarly, the somewhat lower reactivity of $[(L^3{-}2H)Cu_3]^{4+}$ is attributed to the larger energy gap between the ground state and sterically more demanding (and less efficiently stabilized) transition state.

Keywords: Allosterism; Copper; Catalysts; Anion receptor; Phosphodiester cleavage

INTRODUCTION

In many enzymes, two (or more) active site metal ions are involved in selective binding and transformation of the substrate. The design of low-molecular-weight catalysts with synergetic action of two metal centres has been particular successful in the case of metal-promoted phosphoryl transfer reactions [1–3]. Intermetal distance and relative orientation of coordination polyhedra—factors of crucial importance for the cooperative action of two metals—are controlled by the protein backbone in enzymes and by ligand design in their synthetic mimics.

Our own studies in this field include dicopper(II) complexes of macrocyclic ligands and have led to the first transesterification catalyst for highly inert dialkyl phosphates [4] and to the development of a potentiometric anion sensor, based on selective bridging coordination of anions with the appropriate size and shape [5].

Although many dinuclear enzyme mimics have been designed in the past two decades, there is no comprehensive understanding of the relationship between metal-ion preorganization and reactivity. The systematic variation of metal-ion preorganization towards the optimium for a specific reaction is a challenge and requires laborious synthesis of a series of binucleating ligands [6,7]. We have recently introduced a new and versatile strategy to control the spatial organization of two catalytic metal ions without modification of the donor environment: a polypyridyl ligand $\mathbf{L}^1$ was designed which has two bidentate binding sites for functional (catalytic) Cu^{II} ions and an additional site for the binding of a third "structural" metal M_s, which is not directly involved in substrate activation but determines the conformation of the complex (Scheme 1) [8,9]. The two Cu ions cooperate in the catalytic cleavage of a phosphodiester substrate. Reactivity is very much dependent on the nature of the structural metal M_s. Our interpretation is that subtle differences in the ionic radius of M_s and its tendency to form distorted coordination polyhedra have a significant influence on the conformation of the catalyst. Allosteric regulation of catalytic activity—including metal ions as effectors—is commonly observed in enzyme catalysis. The synthetic complexes mentioned above may be considered as prototypes of abiotic allosteric catalysts (although not available with a vacant allosteric site in the absence of the effector M_s). Another allosteric supramolecular catalyst based on a peptide template was described more recently [10].

The aim of the present work was to gain a more detailed understanding of the structural role of an allosteric metal ion in a polynuclear complex. In particular, we were interested to learn, by investigating structures and anion receptor properties, about the accessible conformational space of such a system.

While a high degree of preorganization of multiple functional groups in a receptor is sufficient to achieve a high efficiency and selectivity in binding, a lack of a certain flexibility in a catalyst can give rise to poor efficiency since binding of the substrate and stabilization of the transition state in a dynamic fashion may require significantly different "active site" conformations. This dynamic behaviour is of crucial importance in enzyme catalysis [11]. It was presumed [12] that many enzyme models fail to mimic the high efficiency of enzyme catalysis because they are either too flexible or too rigid in nature.

To address this question, we have focused on copper complexes of the novel tritopic ligand $\mathbf{L}^2$ and have investigated their structure, catalytic activity in phosphoester cleavage and binding of bridging anions of varying size. The topology of $\mathbf{L}^2$ is related to that of $\mathbf{L}^1$, but two pyridyl-N-donors are replaced by amide-N-donors. $\mathbf{L}^2$ is available more readily in pure form and in a larger quantity than $\mathbf{L}^1$ and therefore allows more thorough studies of its metal complexes. The properties of complexes $(\mathbf{L}^2{-}2H)Cu_3$ are compared with those of a closely related ligand $\mathbf{L}^3$ with a reduced conformational flexibility.

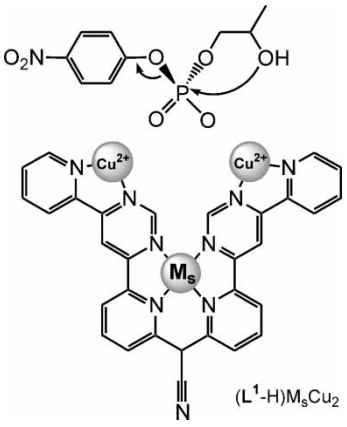

SCHEME 1 Allosteric catalyst for phosphodiester cleavage [8,9].

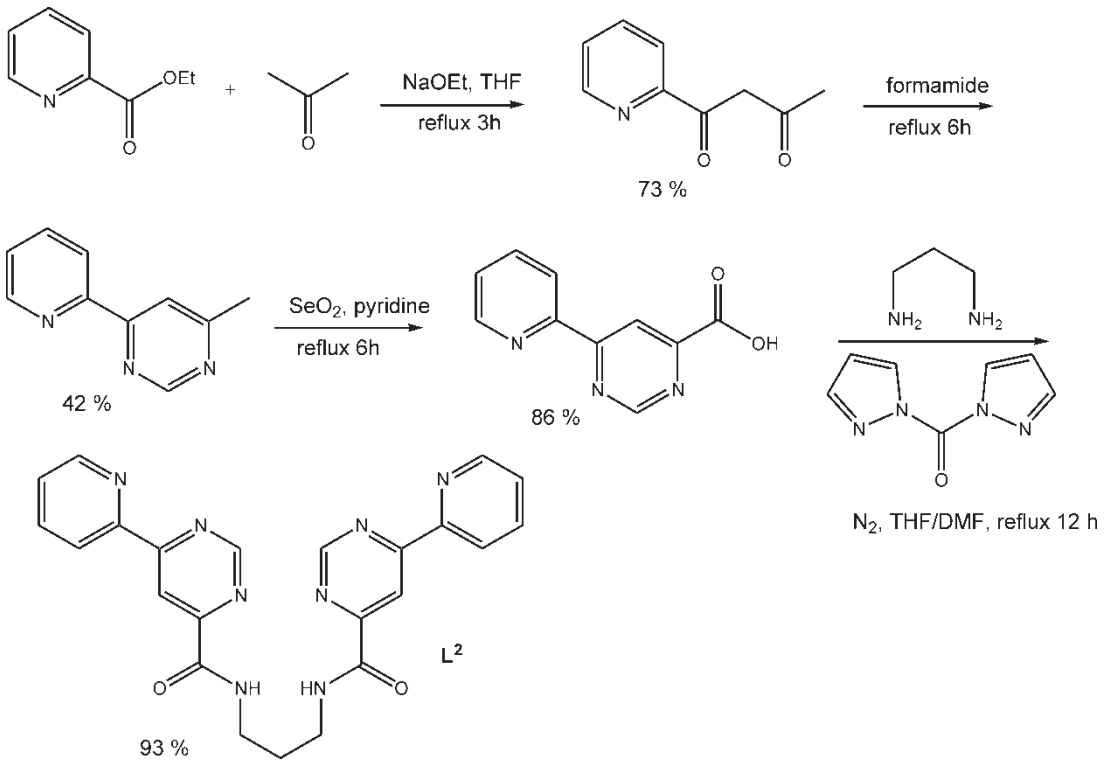

SCHEME 2 Synthesis of $\mathbf{L}^2$.

RESULTS AND DISCUSSION

Ligand Synthesis

$\mathbf{L}^2$ and $\mathbf{L}^3$ were prepared in a four-step synthesis. The precursor 2-methyl-6-(2-pyridyl)-pyrimidine was obtained previously in two steps by condensation of the β-diketone with formamide [13] and was prepared in a modified way with a better overall yield of 30%. SeO_2 oxidation of the methyl group gave the previously unknown 6-(2-pyridyl)-pyrimidine-4-carboxylic acid in 86% yield. $\mathbf{L}^2$ was obtained by reaction of the carboxylic acid (2 equiv.) with 1,3-diaminopropane, using CDI (1,1′-carbonyldiimidazole) as the amide coupling reagent, in a 93% yield after column chromatography on silica (see Scheme 2).

Similarly, $\mathbf{L}^3$ was available using 2-amino-benzylamine, although in a much lower yield (27%).

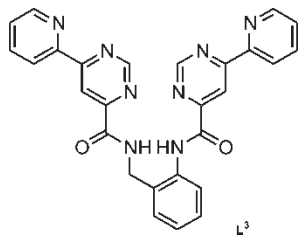

Both ligands could be characterized by ^{1}H-NMR, ^{13}C-NMR, IR spectroscopy and microanalysis. In the infrared spectra of $\mathbf{L}^2$ and $\mathbf{L}^3$, sharp amide(I)-C═O ($\mathbf{L}^2$: 1675 cm^{-1}, $\mathbf{L}^3$: 1672 cm^{-1}) and amide-NH bands ($\mathbf{L}^2$: 3331 cm^{-1}, $\mathbf{L}^3$: 3312 cm^{-1}) are observed.

Crystal Structure of $\mathbf{L}^3$

Colourless single crystals of $\mathbf{L}^3$ were obtained by repeated recrystallization from warm dichloromethane/methanol mixtures. The unit cell contains four symmetry-related molecules; the solid-state structure of $\mathbf{L}^3$ is given in Fig. 1. While intramolecular π−π-stacking is not observed, several intramolecular hydrogen bonds determine the conformation of the molecule. Anilide-N−H interacts with benzylamide-O, and the N···O distance amounts to 2.828(3) Å. A coplanarity of pyrimidine ring and amide group is observed, and both amide-N−H groups are *cis*-oriented relative to the pyrimidine-N, suggesting an interaction by hydrogen bonding [$N_{py}\cdots N_{amide} = 2.658(3)$ Å]. An additional intermolecular hydrogen bond linking amide residues N(31)-H(31N)-O(43)′ [d(D...A) = 2.919(3) Å] and intermolecular π-stacking interactions at 3.5–3.8 Å are relevant for the crystallographic packing of $\mathbf{L}^3$ molecules.

Mononuclear Complexes

A mononuclear copper(II) complex of $\mathbf{L}^2$ was prepared as follows: $\mathbf{L}^2$ was dissolved in

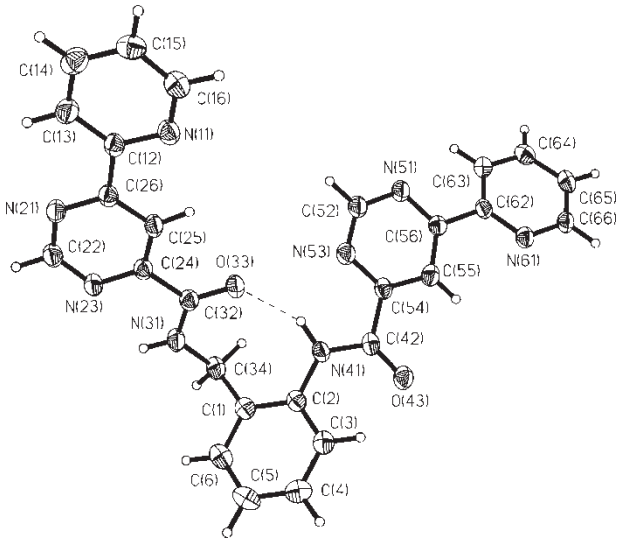

FIGURE 1 Molecular structure and numbering scheme for $\mathbf{L}^3$. Selected bond lengths [Å] and torsion angles [°]: O(33)–C(32) 1.230(3), O(43)–C(42) 1.231(3), N(11)–C(12)–C(26)–N(21) 175.3(2), N(23)–C(24)–C(32)–O(33) 177.7(2), C(32)–N(31)–C(34)–C(1) 78.8(3), N(31)–C(34)–C(1)–C(2) −104.0(3), C(34)–C(1)–C(2)–N(41) 4.9(4), C(2)–N(41)–C(42)–O(43) −0.7(4), O(43)–C(42)–C(54)–N(53) 179.8(2), N(51)–C(56)–C(62)–N(61) 161.8(2).

dichloromethane/DMSO, and a solution of copper(II) chloride (1 equiv.) in water and subsequently aqueous NaOH (2 equiv., to promote deprotonation of amide-NH) were added. After 3 days at room temperature, reddish brown crystals of ($\mathbf{L}^2$–2H)Cu (**1**) were formed. The strong amide C═O infrared band is shifted to lower wavenumbers in the complex (1591 cm^{-1}), confirming Cu coordination by both deprotonated amide nitrogens.

The EPR spectrum of **1** in frozen DMSO solution (139 K), $g_\perp = 2.07$, $g_\parallel = 2.23$, $A_\parallel = 188$, is similar to that of $[(\mathbf{L}^1\text{–H})\text{Cu}]^+$, with a poor resolution due to intermolecular interactions [9]. EPR parameters are typical for in-plane N_4-coordination of Cu^{II} by two amide-N and two neutral N-donors [14].

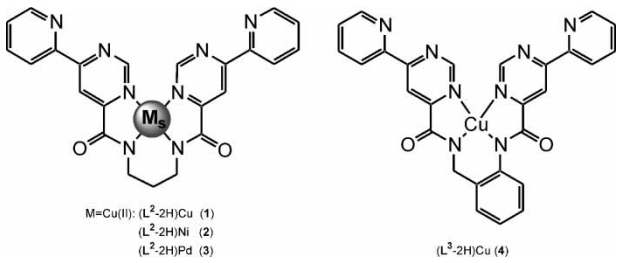

The corresponding orange nickel(II) complex ($\mathbf{L}^2$–2H)Ni (**2**) was obtained in a similar fashion from $\mathbf{L}^2$ and $NiCl_2$ on prolonged heating to 50°C as an orange solid. In the IR spectrum of **2**, a strong amide C═O band at 1597 cm^{-1} indicates Ni-coordination to the deprotonated amide nitrogens. A square planar coordination of low-spin Ni^{II} is most likely, as proven by X-ray crystallography of the Ni^{II} complex of *N*,*N*′-dipicolinyl-1,3-propanediamine, in which the pyrimidyl donor of $\mathbf{L}^2$ is replaced by pyridyl [15]. A more comprehensive characterization of **2** was complicated by the low solubility of the isolated complex; even in warm DMSO, it was only poorly soluble.

The same problem arose with the corresponding yellow palladium(II) complex, prepared from $\mathbf{L}^2$ and $[Pd^{II}(CH_3CN)_4](BF_4)_2$ and isolated as a yellow precipitate. For ($\mathbf{L}^2$–2H)Pd (**3**), a structure analogous to **1** and **2** is proposed on the basis of the infrared spectrum (coord. amide C═O: 1596 cm^{-1}) [15]. Microanalysis is consistent with the presence of one H_2O solvate molecule.

The smooth formation of complexes **1**, **2** and **3** in dilute DMSO solution is demonstrated by a spectrophotometric titration of $\mathbf{L}^2$ with M^{2+} salts in the presence of 2 equiv. of NaOH, following the increasing absorbance of the MN_4 chromophore at about 400 nm. As an example, the titration (Fig. 2) and absorbance diagram (Fig. 3) of the Cu^{II} complex are given. In case of Ni and Pd, complex formation is slow, and harsh conditions had to be applied (30 min at 100°C after each addition of each portion of metal salt) to achieve quantitative formation of ($\mathbf{L}^2$–2H)M.

A mononuclear copper(II) complex of $\mathbf{L}^3$, ($\mathbf{L}^3$–2H)Cu (**4**), was prepared in a similar manner as described for **1**. Spectroscopic data, infrared C═O bands at 1582 and 1599 cm^{-1} for coordinated anilide and amide, EPR parameters in DMSO (298 K) $g_\perp = 2.08$, $g_\parallel = 2.24$, $A_\parallel = 187$ G, LDI mass spectrum [m/z (LDI^+) = 548.4 (calc. for ($\mathbf{L}^3$–2H)^{63}Cu: 549.1)] and microanalysis are consistent with a tetradentate N_4-coordination by two deprotonated amide N-atoms and two pyrimidine N-atoms.

Formation of the corresponding Ni^{II} and Pd^{II} complexes is indicated by IR and UV–Vis spectroscopy, but we were unable to isolate the complexes in an analytically pure form. Again, the complexes were very poorly soluble in common solvents.

Crystal and Molecular Structure of ($\mathbf{L}^2$–2H)Cu (1)

The mononuclear complex is shown in Fig. 4 and has a helical conformation with twofold axial symmetry (the copper atom was found to occupy a special position on the C_2 axis). The extent of the helical twist, described in terms of the value of the dihedral angle between the pyrimidine rings 26.1(9)°, is somewhat greater than that seen in the structure of $[(\mathbf{L}^1\text{–H})\text{Cu}]^+$ [9], where this angle was found to be 18.5(2)°. Consequently, the C(22)–H···H–C(22a) separation between the proximate pyrimidine protons in the present case is about 0.1 Å larger (2.27 Å) than in the previously studied complex.

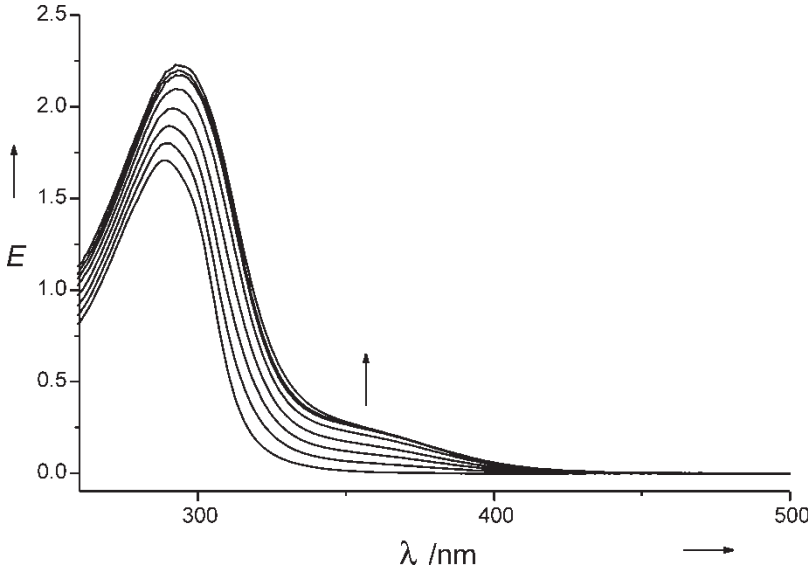

FIGURE 2 Spectrophotometric titration of $\mathbf{L}^2$ (5×10^{-5} M) with copper(II) nitrate in DMSO solution containing 2 equiv. NaOH, $T = 25$°C. Spectra correspond to addition of Cu in 0.2 equiv. steps (0–1.4 equiv. Cu).

The central atom is situated in the distorted square-planar surroundings of four nitrogen atoms belonging to the pyrimidine rings and the deprotonated amide groups. The $Cu-N_{pym}$ distances [Cu(1)–N(23) = 2.015(2) Å] are significantly longer than $Cu-N_{amide}$ [Cu(1)–N(31a) = 1.916(2) Å]. The CuN_4 moiety is subjected to the noticeable tetrahedral distortion: the nitrogen atoms are displaced by 0.232(1) and 0.252(1) Å from their mean plane, while the copper ion lies in this plane due to symmetry reasons. The angle between the coordinated pyrimidine nitrogens N(23)–Cu(1)–N(23a) is 100.8°, resulting in a separation between the external non-coordinated pyrimidine N atoms N(21) and N(21a) of 5.450 Å.

The six-membered chelate ring adopts a twisted envelope conformation with the C(1) atom deviating by 0.198(3) Å from the mean plane of the five other atoms.

Two structures (a and b form) of copper(II) complexes of the related ligand *N*,*N*′-dipicolinyl-1,3-propanediamine with tetradentate coordination by two deprotonated amide-N and two pyridyl-N-atoms, have been described [16–18]. In both structures, an apical water molecule is coordinated to the metal (Cu–O 2.37 Å and 2.27 Å), and Cu-N bond distances (average $Cu-N_{amide}$ 1.95 Å, $Cu-N_{py}$ 2.05 Å) are somewhat longer than in **1**. Cu is located 0.26 Å and 0.24 Å above the plane defined by the four N-donors. Consequently, the conformation of

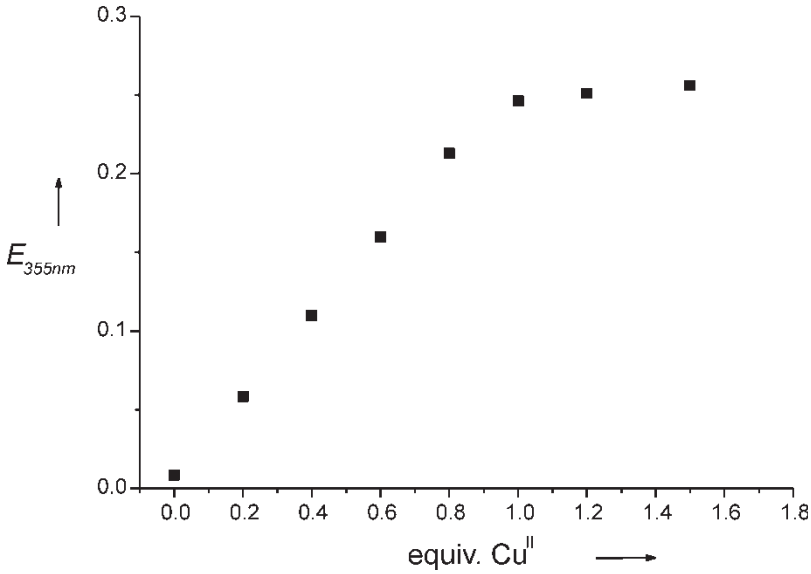

FIGURE 3 Increase in 355 nm absorbance on photometric titration of $\mathbf{L}^2$ with copper(II) nitrate as described for Fig. 2.

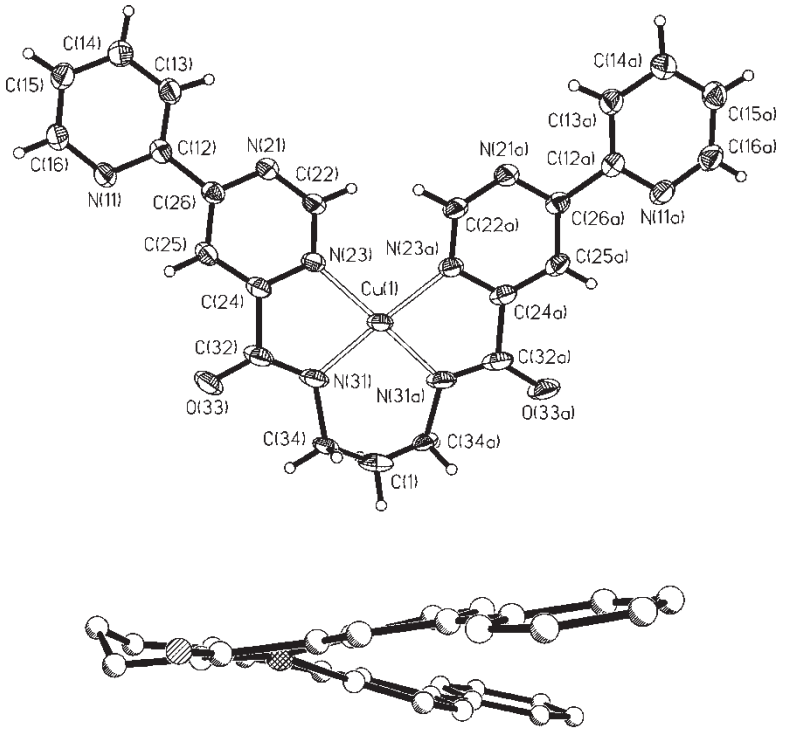

FIGURE 4 Molecular structure and numbering scheme for **1** (top). Side view of **1** (bottom). Selected bond lengths [Å] and angles [°]: Cu(1)–N(31a) 1.9158(16), Cu(1)–N(23a) 2.0145(16), N(31a)–Cu(1)–N(31) 97.15(10), N(31)–Cu(1)–N(23a) 165.69(7), N(31a)–Cu(1)–N(23a) 82.80(7), N(23a)–Cu(1)–N(23) 100.78(9).

the tetradentate site is roof-like in both cases and very different from that found for **1** but similar to that observed in the oxalate complex of $(\mathbf{L}^2\text{–}2H)Cu_3$ (**5**; see below). The intramolecular contact between the two *ortho*-H atoms of the pyridyl groups is much shorter (1.95 Å and 1.86 Å) than that of the corresponding pyrimidyl H-atoms in **1**.

Trinuclear Complexes

Changes in absorbances of $(\mathbf{L}^2\text{–}2H)Cu$ (10^{-4} M in water:DMSO 3:1) on addition of excess Cu^{II} are less significant and do not give as clear an indication of the formation of polynuclear complexes. However, in the presence of the bridging coligands oxalate and phosphate which strongly stabilize the trinuclear complexes (see below), the absorbance diagram at 357 nm (Fig. 5) is compatible with the formation of trinuclear complexes on addition of about 3 equiv. Cu^{2+}. Also, it was possible to isolate an oxalate complex containing the $(\mathbf{L}^2\text{–}2H)Cu_3$ moiety (see below).

Furthermore, kinetic diagrams for phosphodiester cleavage rate at increasing Cu concentration are compatible with the formation of a trinuclear active species in solution, although excess Cu is required for quantitative complex formation.

When 2 equiv. NaOH and 3 equiv. $CuCl_2$ in water are added to a solution of $\mathbf{L}^2$ in dichloromethane/methanol, followed by aqueous sodium oxalate (0.5 equiv.), a dark green solution is obtained. On prolonged standing at room temperature, dark green single crystals of complex 5 form. The most intense band of the infrared spectrum is rather broad and centred at 1610 cm^{-1}, located at a lower frequency than that of bridging and chelating oxalate in the $Cu^{II}(\mu\text{-}\eta_4\text{:}\eta_4\text{-}C_2O_4)Cu^{II}$ moiety at about 1650 cm^{-1} in other complexes [16–18]. A shoulder at 1590 cm^{-1} is attributed to N-coordinated amide C═O. The EPR spectrum of polycrystalline 5 at 120 K is anisotropic with broad signals $g_\perp = 2.07$ and $g_\parallel = 2.22$. In methanolic solution, the ESI mass spectrum of 5 shows a triply positive charged ion peak at m/z (ESI^+) = 1023.5, corresponding to the dodecanuclear complex with three of the coordinated Cl^- ions replaced by CH_3OH (calculated most abundant isotope peak of $[C_{99}H_{92}Cl_5Cu_{12}N_{32}O_{25}]^{3+}$: 1022.9, correct isotope pattern). MALDI-MS spectra show only the mononuclear fragment $[(\mathbf{L}^2\text{–}2H)Cu + H]^+$.

Attempts to prepare trinuclear complexes $[(\mathbf{L}^2\text{-}2H)NiCu_2]^{4+}$ in DMSO solution failed due to the rapid Cu–Ni exchange at the tetradentate site in DMSO solution, evident by spectrophotometry. This behaviour contrasts with that of $[(\mathbf{L}^1\text{–}H)NiCu_2]^{5+}$, where less than 5% exchange is observed in solution after several days. Studies of the trinuclear complexes $[(\mathbf{L}^2\text{–}2H)PdCu_2]^{4+}$ were complicated by the very poor solubility of $(\mathbf{L}^2\text{–}2H)Pd$ (**3**) in aqueous media.

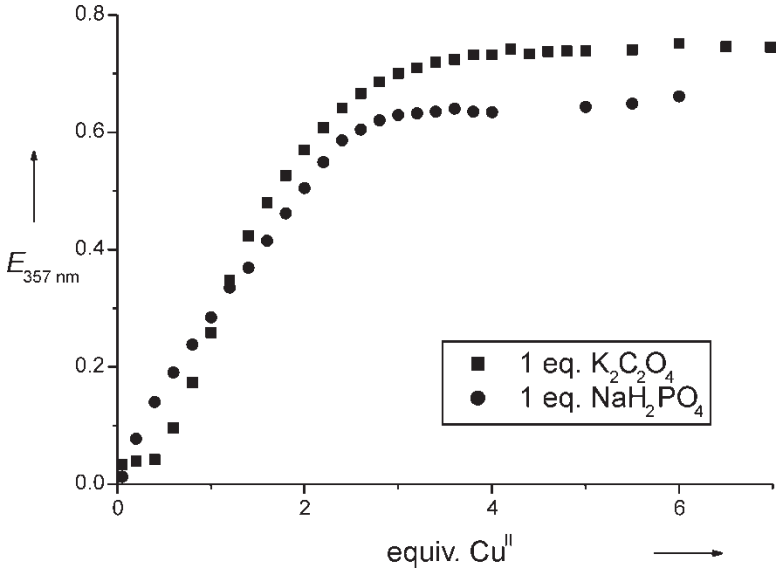

FIGURE 5 Spectrophotometric titration of $\mathbf{L}^2$ (10^{-4} M) with copper(II) nitrate in water:DMSO 3:1 at pH 6.8 [buffer 20 mm 3-(*N*-morpholino)propanesulfonic acid (MOPS), $T = 25°C$] in the presence of $K_2C_2O_4$ or NaH_2PO_4. Increase in absorbance at 357 nm.

Crystal and Molecular Structure of $[(\mathbf{L}^2{-}2H)_4Cu_{12}(\mu_4\text{-}C_2O_4)_2(\mu\text{-}OH)_4(\mu\text{-}Cl)_4Cl_4(H_2O)_2]\cdot 34.83H_2O$ (5)

The unit cell contains eight symmetry-related, neutral molecules of **5** (Fig. 6) which do not have any intrinsic symmetry. Four $(\mathbf{L}^2{-}2H)Cu_3$ units assemble with bridging anions oxalate, chloride and hydroxide to the nanometre-sized dodecanuclear complex. All Cu^{II} ions display tetragonal in-plane coordination with four short coordinative bonds, and one or two additional weak axial contacts. There are two types of copper ions in the complex: four occupying the interior tetradentate N_4 sites of $\mathbf{L}^2$, and eight bound to the external, bidentate py-pym unit.

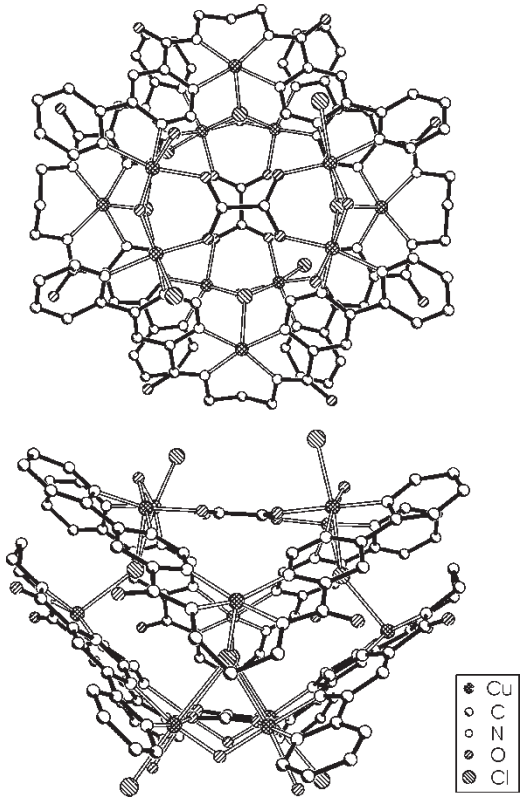

FIGURE 6 Different views of the molecular structure of **5**.

5 is composed of two $(\mathbf{L}^2Cu_3)_2$ pairs which are connected by weak axial contacts of Cu to bridging chloride ions. Within a $(\mathbf{L}^2Cu_3)_2$ pair, the $\mathbf{L}^2Cu_3$ units are connected more tightly, in-plane coordination of the external Cu ions is complemented by bridging oxalate and two OH^- coligands, while two $\mathbf{Cl}^-$ ions form additional axial bridges. The μ_4-bridging coordination mode of oxalate without chelation is unusual for transition metals but has been observed before for 4d and 5d metal ions [19–21]. The $[(\mathbf{L}^2\text{-}2H)Cu_3](\mu_4\text{-}C_2O_4)(\mu\text{-}OH)_2(\mu\text{-}Cl)_2$ $[(\mathbf{L}^2\text{-}2H)Cu_3]$ unit has a roof-like structure, dihedral angles of the two N_4 equatorial planes of the structural Cu ions being 74° (Fig. 6, bottom).

In view of the relevance of the conformational flexibility at the allosteric Cu site for guest binding and catalysis by $[(\mathbf{L}^2{-}2H)Cu_3]^{4+}$, it is of particular interest to compare the structures of the (symmetry-independent) $(\mathbf{L}^2{-}2H)Cu_3$ units in **5** (Fig. 7) and the mononuclear complex $(\mathbf{L}^2{-}2H)Cu$ (**1**) (Fig. 4). In helically twisted **1**, the CuN_4 unit is tetrahedrally distorted, but Cu is located in the best plane of N atoms. The conformation of $(\mathbf{L}^2\text{-}2H)Cu$ units in **5** is principally different: they adopt a butterfly-like conformation (Fig. 7, bottom), with both py-pym wings bent to the same side of the CuN_4 plane with dihedral angles between the two pyrimidine rings in the range 29–35°. The Cu ions are noticeably raised

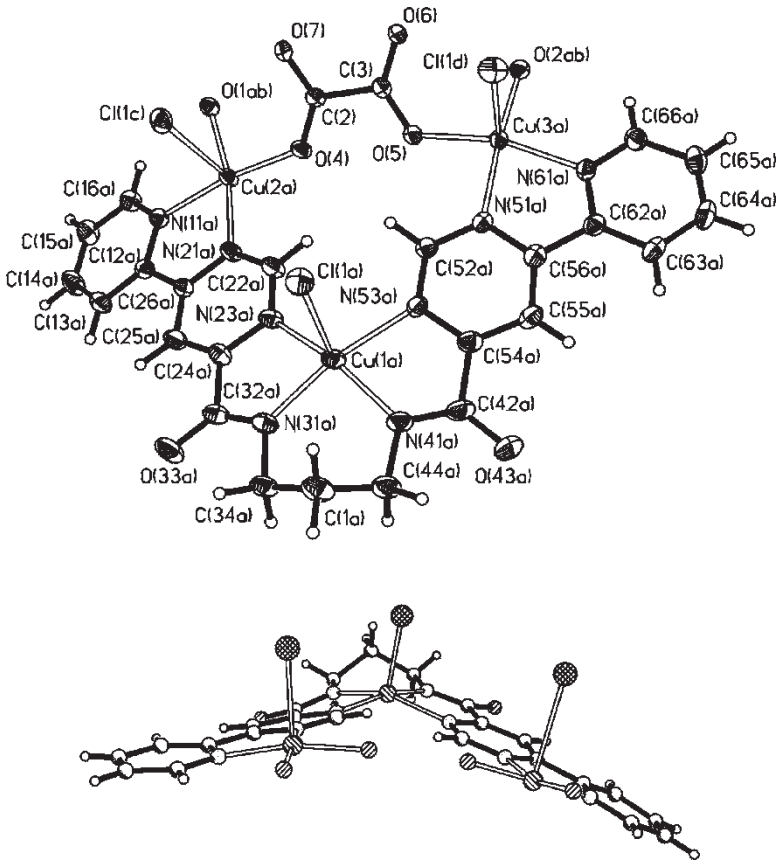

FIGURE 7 ($\mathbf{L}^2$–2H)Cu_3(μ-C_2O_4)(μ-$OH)_2$-subunit of **5**, structure and numbering scheme (top). Different view of the same subunit, for clarity only the donors O(4) and O(5) of the bridging oxalate are shown (bottom). Selected bond lengths (Å) and angles (°): Cu(1a)–N(41a) 1.959(4), Cu(1a)–N(53a) 2.113(3), Cu(1a)–Cl(1a) 2.4749(13), Cu(1a)–Cu(2a) 6.1756(7), Cu(1a)–Cu(3a) 6.2022(7), Cu(3a)–Cu(2a) 6.4484(7), Cu(3a)–O(2ab) 1.922(3), Cu(3a)–O(5) 1.945(3), Cu(3a)–N(61a) 2.002(3), Cu(3a)–N(51a) 2.033(3), Cu(3a)–Cl(1d) 2.5549(12), N(31a)–Cu(1a)–N(41a) 92.83(15), N(31a)–Cu(1a)–N(23a) 80.08(14), N(23a)–Cu(1a)–N(53a) 101.26(13), O(2ab)–Cu(3a)–O(5) 94.06(13), O(2ab)–Cu(3a)–N(61a) 94.90(14), O(5)–Cu(3a)–N(61a) 162.15(14), O(2ab)–Cu(3a)–N(51a) 173.36(14), O(5)–Cu(3a)–N(51a) 89.14(13), N(61a)–Cu(3a)–N(51a) 80.49(14).

from the N_4 mean plane by 0.20–0.33 Å, and they all have one or two weak contacts to axial Cl^- or H_2O ligands. The proximal pyrimidine hydrogens come closer, C_{pym}–H···H–C_{pym} 2.08–2.15 Å, than in **1** (2.27 Å). Compared with **1**, an elongation of the coordinative in-plane bonds of the structural Cu ions in **5** is observed. In particular, the Cu–N_{pym} bonds are stretched by 0.07–0.11 Å (Cu–N_{amide} distances by 0.03–0.045 Å). This leads to an increased separation of the external pyrimidine N atoms N(21)···N(51) by 0.38–0.39 Å relative to **1**. The distance between the functional Cu ions within ($\mathbf{L}^2$-2H)Cu_3 is in the range 6.39–6.47 Å. Apparently, to adopt the requirements of the bridging oxalate guest, the coordination sphere of the structural Cu ion in **5** undergoes significant conformational changes with respect to **1** and is more similar to that observed in the Cu^{II} complexes of *N*,*N*′-dipicolinyl-1,3-propanediamine [22–25].

The 1,4-O,O bridging mode of oxalate is preferred over the alternative 1,3-O,O mode which is often observed for monocarboxylates. The 1,3-O···O distance (2.24-2.25 Å) is much shorter than the 1,4-O···O distance (2.63–2.64 Å), and the 1,3-bridging mode requires a much smaller Cu···Cu separation than that observed in **5**. The steric repulsion of the two proximate pyrimidine-H atoms should define a lower limit for the Cu···Cu separation, possibly disfavouring the 1,3-bridging mode of carboxylate.

Catalytic Phosphodiester Cleavage

We have examined the reactivity of the copper complexes of $\mathbf{L}^2$ and $\mathbf{L}^3$ towards the RNA analogue 2-hydroxypropyl-4-nitrophenylphosphate (HPNP). Intramolecular cyclization of this phosphodiester (Scheme 3) is easily followed photometrically by the 400 nm absorbance of released nitrophenolate.

Kinetic studies at varying Cu concentrations were performed in a buffered water:DMSO 3:1 mixture at pH 6.8, 0.1 mM $\mathbf{L}^2$ ($\mathbf{L}^3$, respectively) and 0.5 mM HPNP. Initial rates of cleavage were recorded (Fig. 8).

At Cu concentrations <0.3 mM (<3 equiv. with respect to $\mathbf{L}^n$), precipitation of the mononuclear complex occurred. Maximal activity is reached at

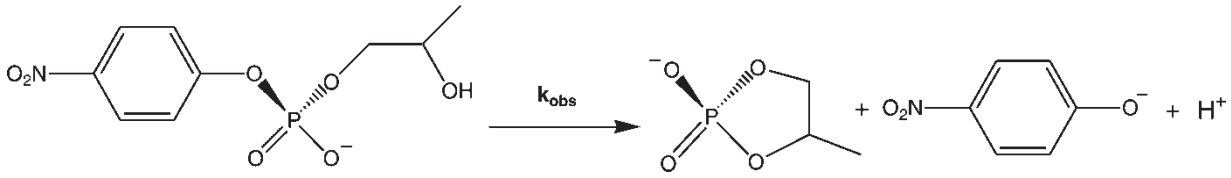

SCHEME 3 Intramolecular cleavage of the phosphodiester 2-(hydroxypropyl)-*p*-nitrophenyl phosphate (HPNP).

about 0.5 mM Cu, indicating that excess copper (5 equiv.) is necessary for the quantitative formation of $[(\mathbf{L}^2\text{-}2H)Cu_3]^{4+}$ and $[(\mathbf{L}^3-2H)Cu_3]^{4+}$, respectively, as observed previously for the tricopper complex of $\mathbf{L}^1$ under the same conditions [9]. Catalysis by free Cu^{2+} ions is negligibly slow ($k_{obs} \approx 10^{-6}\,s^{-1}$). A slight decrease in activity at Cu concentrations >0.5 mM may be explained by competitive binding of the HPNP substrate by free Cu^{2+}. Kinetic data at Cu concentrations <0.3 mM were available in a 1:1 water:DMSO solvent mixture. ($\mathbf{L}^2$–2H)Cu, formed quantitatively at a 1:1 copper:ligand ratio, is inactive for HPNP cleavage, but activity increases on addition of more Cu, reaching $k_{obs} = 1.9$ ($10^{-4}\,s^{-1}$ at 4.5 equiv. Cu).

Further kinetic studies have been performed using a 0.1 mM ligand ($\mathbf{L}^2$, $\mathbf{L}^3$) and 0.5 mM copper(II) nitrate concentration, assuming that the trinuclear complex $[(\mathbf{L}^n-2H)Cu_3]^{4+}$ is formed quantitatively and present at 0.1 mM concentration.

The pH dependence of HPNP cleavage was investigated in the pH range 6.5–7.2. (Fig. 9). $[(\mathbf{L}^2-2H)Cu_3]^{4+}$ and $[(\mathbf{L}^3-2H)Cu_3]^{4+}$ display a similar dependence of k_{obs} on pH and have maximal reactivity at pH 6.8. A reasonable explanation is competitive binding of the substrate HPNP and of OH^- to the free sites of the functional Cu ions. A Cu-coordinated hydroxide (pK_a of about 7 is typical for Cu-coordinated water) may be essential for the catalytic activity of the complex, but at high pHs, free sites at both functional Cu are blocked by OH^-, and the reactivity decreases. A reaction mechanism in which free OH^- acts as a general base and deprotonates the alcohol group of HPNP is not consistent with the observed pH rate profile, since one would expect a more pronounced increase in rate with OH^- concentration.

The temperature dependence of k_{obs} at pH 6.8 in the range 15–35°C follows Arrhenius's law, with a doubling of k_{obs} with increase in temperature by 10°C.

The dependence of reaction rate on HPNP concentration was explored in the range 0.2–2.5 mM substrate at a complex concentration of 10^{-4} M, pH 6.8 and 25°C (Fig. 10). At HPNP concentrations >3 mM, some decrease in reactivity is observed (e.g. at 5 mM HPNP dc/dt is 90% of the value at 3 mM) instead of the plateau expected for perfect Michaelis–Menten behaviour. Again, a rational explanation is competition of substrate and hydroxide for coordination to Cu, and a high reactivity is only achieved if both HPNP and OH^-

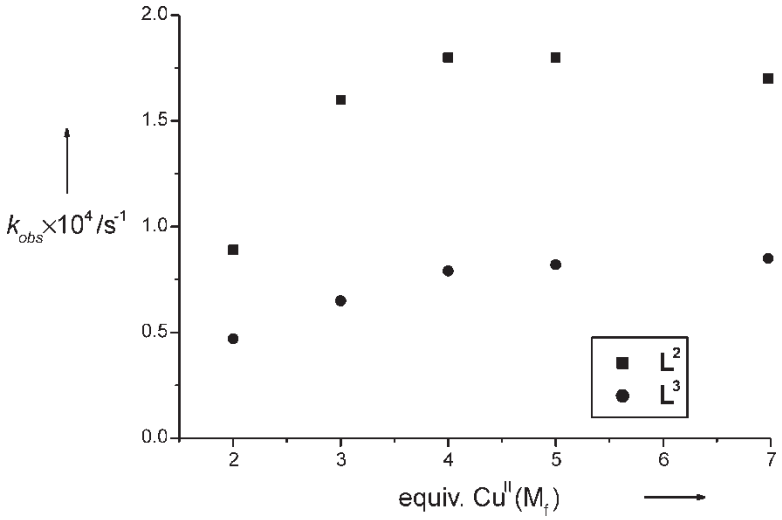

FIGURE 8 k_{obs} for cleavage of HPNP (5×10^{-4} M) by 10^{-4} M [($\mathbf{L}^n$–2H)Cu] ($n = 2, 3$) at varying copper(II) nitrate concentrations. Water:DMSO 3:1, pH 6.8, buffer 20 mm 3-(*N*-morpholino)propanesulfonic acid (MOPS), $T = 25$°C. Average values of three kinetic runs, reproducible within ±15%.

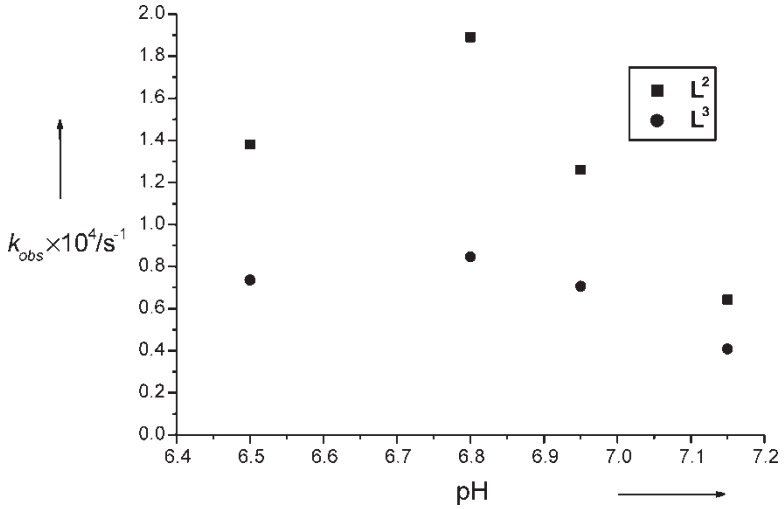

FIGURE 9 pH dependence of k_{obs} for the cleavage of HPNP (5×10^{-4} M) by 10^{-4} M $[(\mathbf{L}^n{-}2H)Cu_3]^{4+}$ ($n = 2, 3$), prepared in situ from $\mathbf{L}^n$ and 5 equiv. Cu. Water:DMSO 3:1, $T = 25$°C, buffers: 20 mm 3-(*N*-morpholino)propanesulfonic acid (MOPS, pH 6.8–7.2) or 20 mm 2-(*N*-morpholino)ethanesulfonic acid (MES, pH 6.5). Average values of three kinetic runs, reproducible within ± 15%.

are coordinated to $[(\mathbf{L}^n{-}2H)Cu_3]^{4+}$. At a high [HPNP], an unproductive species $\mathbf{L}Cu_3(HPNP)_2$ containing a second (more weakly bound) HPNP may form. A Michaelis–Menten analysis has been performed on the assumption that the concentration of this species is negligible at [HPNP] < 2.5 mM.

A Lineweaver–Burk plot (Fig. 11) illustrates the linear dependence of reciprocal rate $(dc/dt)^{-1}$ on reciprocal substrate concentration for the HPNP concentration range 0.2–2.5 mM.

From the plots in Fig. 11, the values of k_{cat} (first-order rate constant for the cleavage of HPNP when bound to the catalyst) and of K_m (Michaelis constant) were derived (Table I). $K_{HPNP} = (K_m)^{-1}$ corresponds to the equilibrium constant for binding of HPNP to $[(\mathbf{L}^n{-}2H)Cu_3]^{4+}$. While $[(\mathbf{L}^2{-}2H)Cu_3]^{4+}$ cleaves bound HPNP about three times faster than $[(\mathbf{L}^3{-}2H)Cu_3]^{4+}$, the latter complex binds this substrate about 1.6 times more efficiently.

An important structural difference of the otherwise very similar ligands $\mathbf{L}^2$ and $\mathbf{L}^3$ is the three-atom linkage between the amide nitrogens, $-CH_2CH_2CH_2$ in $\mathbf{L}^2$ and a more rigid $-CH_2CH{=}CH$ moiety in $\mathbf{L}^3$. This should result in a decreased conformational flexibility of complexes of the latter ligand.

The kinetic parameters for the trinuclear complex $[(\mathbf{L}^2{-}2H)Cu_3]^{4+}$ are similar to those found for $[(\mathbf{L}^1{-}H)Cu_3]^{5+}$ under the same conditions [9]; in

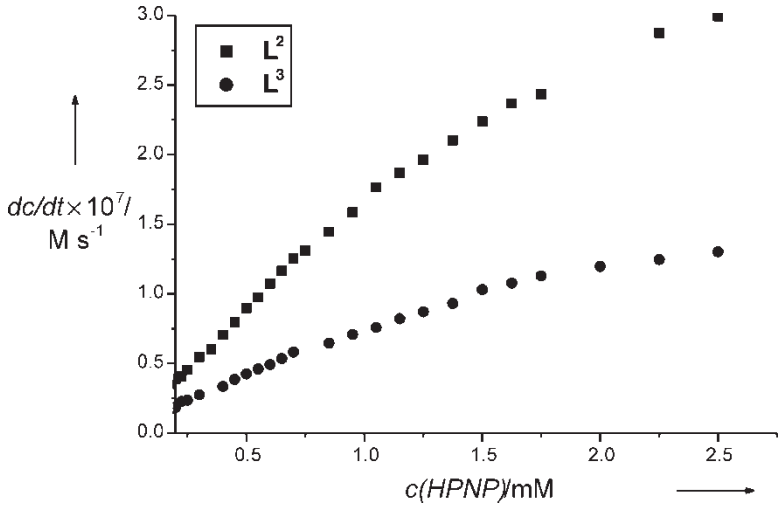

FIGURE 10 Rate (dc/dt) of HPNP cleavage by 10^{-4} M $[(\mathbf{L}^2{-}2H)Cu_3]^{4+}$ or $[(\mathbf{L}^3{-}2H)Cu_3]^{4+}$ at varying substrate concentrations. Water:DMSO 3:1, pH 6.8, buffer 20 mm 3-(*N*-morpholino)propanesulfonic acid (MOPS), $T = 25$°C. Average values of three kinetic runs, reproducible within ± 15%.

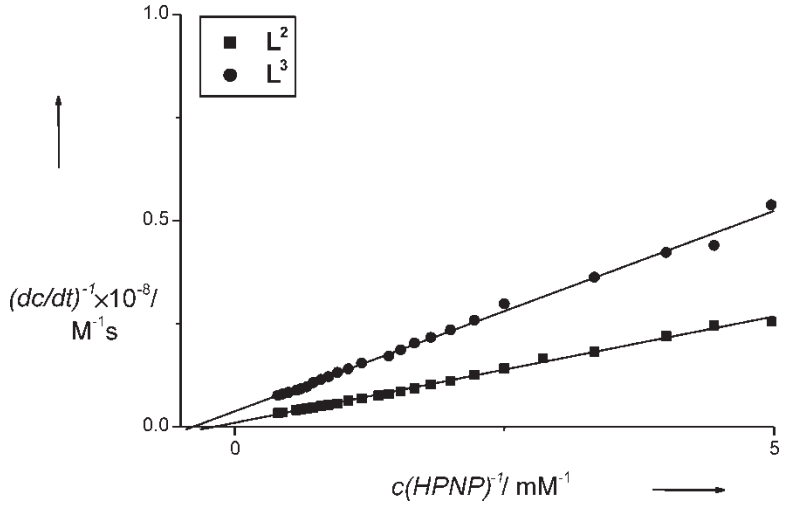

FIGURE 11 Lineweaver–Burk plot for catalytic HPNP cleavage, dependence of $(dc/dt)^{-1}$ on $[HPNP]^{-1}$ derived from Fig. 10.

this case, a comparative discussion of the reactivities in terms of the conformational aspect is complicated by the higher overall charge of $[(\mathbf{L}^1\text{–H})Cu_3]^{5+}$, which should have a positive influence on reactivity owing to increased Lewis acidity of the functional Cu ions.

Competitive Anion Binding

We have screened the ability of various anions to inhibit catalytic HPNP cleavage by complexes $[(\mathbf{L}^n\text{–2H})Cu_3]^{4+}$ and have attributed this effect to competitive binding of the anion to the catalytic dicopper site. A non-competitive inhibition by interaction of the inhibitor with the allosteric Cu ion appears unlikely since the central Cu ion is expected to retain its stable in-plane N_4-coordination, and additional interaction with anions via axial sites should be weak and irrelevant in dilute solution. Owing to the above-mentioned complications at high HPNP concentrations, it was not possible to directly confirm the constancy of v_{max} in the presence of inhibitors by applying a large excess of HPNP.

Abstraction of functional Cu ions from $[(\mathbf{L}^n\text{–2H})Cu_3]^{4+}$ by competitive complex formation is readily ruled out for many anions in view of their small Cu^{2+} binding constants. For others, strong inhibition at a 1:1 inhibitor:$[(\mathbf{L}^n\text{–2H})Cu_3]^{4+}$ ratio is not consistent with simple complexation of 1 equiv. Cu, since experiments have been performed at a **L**/Cu 1/5 ratio.

Figure 12a shows strong inhibitors which lower the catalytic rate by >50% when present in 0.5 mM concentration (= 5 equiv. relative to $\mathbf{L}^n$ and 1 equiv. relative to HPNP). v_{rel} corresponds to the ratio v/v_0, when v is the observed rate for HPNP cleavage in the presence and v_0 in the absence of inhibiting anion. v_{rel} is monitored at varying inhibitor concentrations for both $[(\mathbf{L}^2\text{–2H})Cu_3]^{4+}$ (closed symbols) and $[(\mathbf{L}^3\text{–2H})Cu_3]^{4+}$ (open symbols). In Fig. 12b, a series of less effective inhibitors is presented. The cleavage rate is unchanged on addition of 5 mM Cl^-, NO_3^-, ClO_4^- and BF_4^- (Na^+ or K^+ salts). This observation confirms that a subtle increase in ion strength

TABLE I Catalytic cleavage of HPNP by catalyst $[(\mathbf{L}^n\text{–2H})Cu_3]^{4+}$, values of K_{HPNP} (formation constant of catalyst–HPNP complex) and of k_{cat} (rate constant for the cleavage of catalyst-bound HPNP), derived from the Lineweaver–Burk plot in Fig. 11

Catalyst	K_{HPNP}, M^{-1}	k_{cat}, s^{-1}
$[(\mathbf{L}^2\text{–2H})Cu_3]^{4+}$	190	10×10^{-3}
$[(\mathbf{L}^3\text{–2H})Cu_3]^{4+}$	305	3.2×10^{-3}

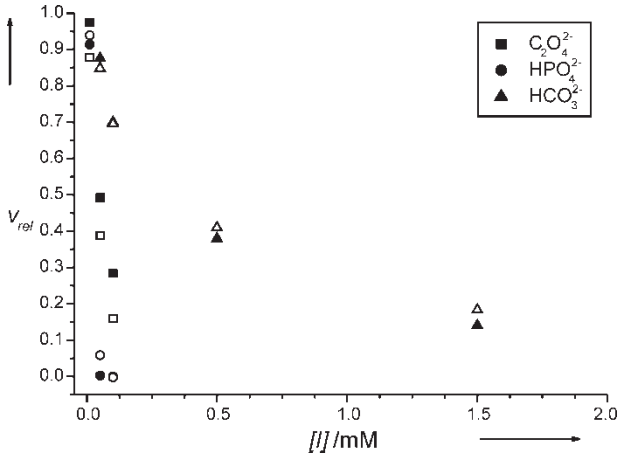

FIGURE 12 Relative rate (v_{rel}) of HPNP cleavage by 10^{-4} M $[(\mathbf{L}^2\text{–2H})Cu_3]^{4+}$ (closed symbols) and $[(\mathbf{L}^3\text{–2H})Cu_3]^{4+}$ (open symbols) in the presence of inhibiting anions at varying concentrations. v_{rel} corresponds to the ratio v/v_0, v is the observed rate for HPNP cleavage in the presence and v_0 in the absence of inhibiting anion. Conditions: water:DMSO 3:1, pH 6.8, buffer 20 mm 3-(*N*-morpholino)propanesulfonic acid (MOPS), $T = 25$°C. Average values of three kinetic runs, reproducible within ± 15%.

TABLE II Anion binding constants, K, for complexes ($\mathbf{L}^n$–2H)Cu_3, and Cu^{2+}, derived from experiments described by Fig. 12*

Anion	K[($\mathbf{L}^2$–2H)Cu_3]	K[($\mathbf{L}^3$–2H)Cu_3]	K(Cu^{2+})†
HPO_4^{2-}	$>10^5$	$>10^5$	10^4 [27]
$C_2O_4^{2-}$	$>10^4$	$>10^4$	$10^{5.4}$ [34]
HCO_3^-	4200	3900	1600 [35]
SO_4^{2-}	1300	3200	63 [36]
ReO_4^-	350	230	<10 [this work]
HPNP	190	305	15‡ [28]
$CH_3CO_2^-$	170	340	79 [26]
F^-	83	99	13 [37]

*K is the average of several K_I values calculated using Eq. (2) at various concentrations of the anion, maximum deviation of $K_I \pm 15\%$ from K. †Values at ion strength $\mu = 0.01$ M. ‡Value at $\mu = 0.5$ M.

($\mu \approx 0.01$ M at 20 mM MOPS buffer) by addition of 5 mM salt does not significantly influence reactivity.

On the assumption [Eq. (1)] of a simple competition model:

$$(\mathbf{L}^n\text{–}2\text{H})Cu_3(\text{HPNP}) + \text{anion} \rightleftarrows (\mathbf{L}^n\text{–}2\text{H})Cu_3(\text{anion}) + \text{HPNP} \quad (1)$$

and using K_m values $5.3 \times (10^{-3}$ M ($\mathbf{L}^2Cu_3$) and 3.3×10^{-3} M ($\mathbf{L}^3Cu_3$), data of Fig. 12 were used to evaluate $\mathbf{L}Cu_3$ binding constants K_I of inhibiting anions I by fitting to the equation:

$$v_{rel} = (1 + K_m[\text{HPNP}]^{-1})/\{1 + K_m[\text{HPNP}]^{-1}(1 + [\text{I}]K_I)\} \quad (2)$$

This term was derived from the standard equation for enzymatic reaction rate in the presence of a competitive inhibitor. A prerequisite for the use of this equation is that HPNP and inhibitor are present in excess relative to the catalyst. In case of strong inhibition at low concentrations of I (phosphate, oxalate), K_I is underestimated. The anion binding constants K given in Table II are average values of the K_I [calculated by Eq. (2)] at various concentrations [I] of the inhibiting anion.

To assess whether anion affinity is related to a more or less perfect fit of the (potentially) bridging anions to the dicopper site, it is not sufficient to consider the values of K_I alone since the anions have very different affinities to Cu^{2+} ions depending, for example, on their basicity. Therefore, in Table II, we have included the literature-reported Cu^{2+} binding constants $K(Cu^{2+})$ of the same anions. In some cases (acetate, phosphate), data for (bpy)Cu^{2+} and (phen)Cu^{2+} were available, too [26,27], and very similar to the values for Cu^{2+} ion. In most cases, literature data were available at the ionic strength of reaction solutions (0.01 M), some values were obtained by extrapolation. If K[($\mathbf{L}^n$–2H)Cu_3] is much larger than $K(Cu^{2+})$, interaction of the anion with both functional Cu ions by bridging coordination is likely.

The HPNP binding constant of ($\mathbf{L}^n$–2H)Cu_3 was put in relation to the affinity constant of ethyl-*p*-nitrophenyl phosphate for the Cu^{II} complex of triazacyclononane, which has two vacant, *cis*-oriented in-plane sites. For the latter complex, $K = 15\,M^{-1}$ at 51°C and $\mu = 0.5$ M was derived by kinetic methods in a careful study [28]; at the lower ion strength $\mu = 0.01$ M of our reaction solutions, a higher value of about $40\,M^{-1}$ is expected [26]. For (2,2′-bipyridine)Cu^{2+} and bis(4-nitrophenyl)-phosphate, an association constant $K = 20\,M^{-1}$ at 75°C and $\mu = 0.1$ M was reported [29] (we are not aware of studies on the temperature dependence of phosphodiester-Cu^{2+} binding constants. For non-chelating anions with charge −1, some decrease in Cu^{2+} binding constant with decreasing temperature is often observed.) Binding constants of [($\mathbf{L}^n$–2H)Cu_3]$^{4+}$ are much higher and comparable with the value $K = 250\,M^{-1}$ reported for bridging coordination of HPNP to a dinuclear copper(II) calixarene complex at 25°C in water:EtOH 3:1, 20 mM buffer [12]. To our knowledge, Cu^{2+} binding constants of perrhenate ReO_4^- have not yet been reported. It should have a very low affinity to metal ions in aqueous solution due to its low basicity [pK_a ($HReO_4$) − 1.3] [30,31]. Since the cleavage rate of HPNP (1 mM) by Cu^{2+} (0.25 mm) at pH 6.8 and 25°C is not lowered by the addition of 2.5 mM perrhenate, the Cu^{2+} binding constant of perrhenate under these conditions was estimated at $<10\,M^{-1}$. A comparison of the Cu^{2+} and ($\mathbf{L}^n$–2H)Cu_3 binding constants of oxalate is complicated by the fact that this anion coordinates as a chelating ligand to Cu^{2+} ions but as a non-chelating, bridging ligand to [($\mathbf{L}^n$–2H)Cu_3]$^{4+}$. A possible explanation for the nearly full inhibition of catalysis at 0.5 equiv. phosphate is the formation of a very stable dimer ($\mathbf{L}^2$–2H)Cu_3(μ-OH)(μ$_4$-PO_4)(μ-OH)Cu_3($\mathbf{L}^2$–2H) in solution, as compared with the ($\mathbf{L}^2$–2H)Cu_3(μ-OH, Cl)(μ$_4$-C_2O_4)(μ-OH, Cl)Cu_3($\mathbf{L}^2$–2H) dimers in **5** in the solid state.

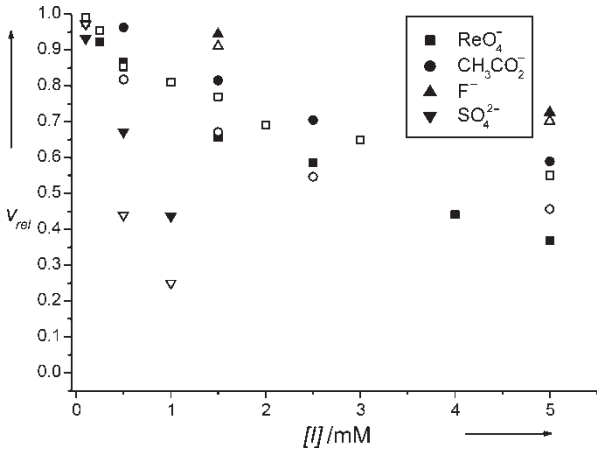

In our view, F^-, the "smallest" anion under consideration, cannot bridge the two functional

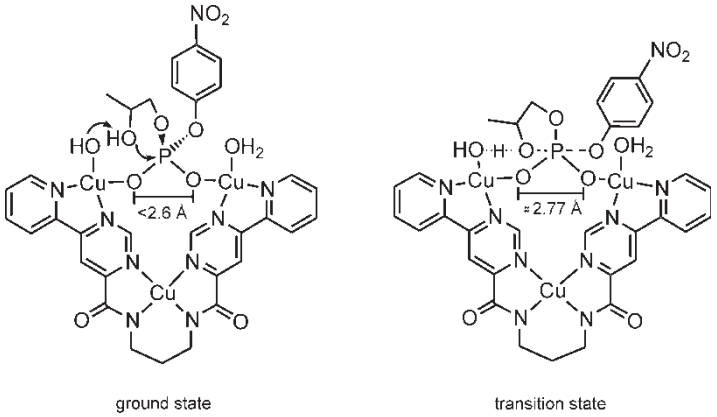

SCHEME 4 Proposed mechanism of HPNP cleavage by $[(\mathbf{L}^n\text{–}2H)Cu_3]^{4+}$, including estimated O···O distances of bridging HPNP in the ground and transition state.

copper ions for steric reasons. Nevertheless, the F^- binding constant, *K*, of $[(\mathbf{L}^n\text{–}2H)Cu_3]^{4+}$ is about seven times larger than of Cu^{2+}. One explanation is the strong tendency of F^- to form hydrogen bonds; in our specific case, we suggest a Cu–F···H_2O–Cu interaction. $[(\mathbf{L}^n\text{–}2H)Cu_3]^{4+}$ binding constants of $CH_3CO_2^-$ and HCO_3^- are only two to four times larger than for Cu^{2+}. In the solid state, the interatomic O···O distance in "free" acetate and hydrogen carbonate is 2.17 and 2.18 Å, respectively—much shorter than the O···O distance of 2.63–2.64 Å in bridging oxalate in compound **5**. $CH_3CO_2^-$ and HCO_3^- are possibly too small for a strain-free bridging coordination.

In contrast, the relatively large tetrahedral anions HPO_4^{2-}, SO_4^{2-} and ReO_4^- have a >10 times higher affinity to the trinuclear complexes than to Cu^{2+}. Since the O···O distance in the free anions (2.45, 2.52, 2.80 Å) is close to the oxalate O···O distance in **5**, a bridging coordination to $[(\mathbf{L}^n\text{–}2H)Cu_3]^{4+}$ appears very likely.

Recently, anion preferences for a dicopper(II) cryptate have been analysed by spectrophotometry and have been similarly interpreted in terms of the "bite length" of the potentially bridging anions [32,33], although the data were not put in relation to the affinities of the anions for free Cu^{2+}. The cryptate appears to have a preference for bridging anions with a somewhat shorter X···Y distance (X, Y = donor atoms of the bridging anion) of 2.3–2.4 Å but is a poor receptor for anions with interatom distance >2.6 Å.

Discussion of the Reaction Mechanism in Context with Anion Binding Constants

A comparison of $[(\mathbf{L}^2\text{–}2H)Cu_3]^{4+}$, and $[(\mathbf{L}^3\text{–}2H)Cu_3]^{4+}$ reveals that the former complex has a preference for "larger" anions such as perrhenate (bite size 2.8 Å), while the latter has a preference for smaller anions (bite size 2.4–2.5 Å). This may be a consequence of the reduced conformational flexibility of $(\mathbf{L}^3\text{–}2H)Cu_3$ ($CH_2CH_2CH_2$ linker is replaced by $CH_2CH{=}CH$), which disfavours a widening of the Cu···Cu distance for incorporation of bridging perrhenate. Also, this effect may be relevant to the different HPNP cleavage reactivities of the complexes. The HPNP binding constants of $(\mathbf{L}^n\text{–}2H)Cu_3$ are about five to eight times higher than the estimated values (extrapolated to 0.01 M ion strength) of mononuclear copper complexes. This is an indication of bridging rather than monodentate coordination. According to the mechanism proposed in Scheme 4, the Cu···Cu separation is expected to increase slightly on stabilization of the transition state.

In crystal structures of phosphodiester bridged dicopper(II) complexes [38,39], the P–O bond distances are in the order of 1.48 Å, similar to the value of "free" phosphodiester. The O–P–O angle is not close to 109° (as expected for an ideal PO_4 tetrahedron) but widens to about 118°. Nevertheless, the O···O distance is <2.6 Å in these complexes.

Ab initio calculations of the trigonal-bipyramidal transition state of dimethyl phosphate methanolysis reveal $P\text{–}O_{equatorial}$ distances in the gas phase of about 1.5 Å [40,41], but coordination of both $O_{equatorial}$ to divalent metal ions such as Mg^{2+} results in a significant lengthening to about 1.6 Å [41]. Given that the $O_{equatorial}\text{–}P\text{–}O_{equatorial}$ angle adopts the ideal value of 120°, the O···O distance in the transition state would be 2.77 Å, very close to the value of ReO_4^-.

On the basis of this consideration, the more efficient binding (by a factor of 1.5) of perrhenate (representing a "transition state analogue" of the HPNP cleavage reaction) by $[(\mathbf{L}^2\text{–}2H)Cu_3]^{4+}$ and the higher affinity (by a factor of 1.6) of $[(\mathbf{L}^3\text{–}2H)Cu_3]^{4+}$ to the substrate HPNP should reflect different ground state-transition state energy gaps for

the two complexes (a larger gap in the case of $[(\mathbf{L}^3-2H)Cu_3]^{4+}$). This would be a sufficient explanation for the approximately three times larger k_{cat} value of $[(\mathbf{L}^2-2H)Cu_3]^{4+}$.

CONCLUSION

Structural, kinetic and anion binding studies have provided an insight into the conformational role of the allosteric Cu ion in the trinuclear catalyst $[(\mathbf{L}^2-2H)Cu_3]^{4+}$:

- Two significantly different low-energy conformations are available: a roof-type structure in which allosteric Cu is located at the top of a square based CuN_4 pyramid, and a helically twisted form in which the CuN_4 polyhedron is tetrahedrally distorted, and the Cu ion lies in the N_4-plane. In the roof-type conformation, the distance of the functional Cu ions in an oxalate bridged complex is 6.4 Å.
- The complexes efficiently bind tetrahedral anions SO_4^{2-}, PO_4^{3-}, HPNP, ReO_4^-, which have a similar "bite size" (O···O 2.5–2.8 Å) to bridging oxalate in **5**. Acetate and hydrogen carbonate (O···O 2.2 Å) are possibly too small for bridging coordination and interact less efficiently with the complexes.
- The proposed reaction mechanism—double Lewis-acid activation of the bridging HPNP substrate by two functional Cu ions of $[(\mathbf{L}^2-2H)Cu_3]^{4+}$, combined with generation of the alcoholate nucleophile by Cu–OH—would involve only minor conformational changes for the conversion of the ground state to a transition state.
- The approximately three times higher reactivity of $[(\mathbf{L}^2-2H)Cu_3]^{4+}$ compared with the related complex $[(\mathbf{L}^3-2H)Cu_3]^{4+}$ is interpreted as a consequence of reduced conformational flexibility of the latter complex, which favours binding of the substrate but disfavours a widening of the Cu···Cu distance for interaction with the transition state.

EXPERIMENTAL

Reagents were obtained from Aldrich Chemical, ACROS Organics, or Fluka Chemie and used as received. Chemicals were of reagent quality, and solvents were of technical grade unless stated otherwise. Organic syntheses in dry solvents were carried out under nitrogen using the Schlenk technique. Workup was performed in technical-grade solvents. The barium(II) salt of 2-hydroxypropyl-*p*-nitrophenyl-phosphate was prepared following a previously reported method [42]. Preparative column chromatography was carried out on Merck 60 silica gel (0.040–0.063 mm). Retention factors (R_f) were determined using Macherey–Nagel alumina TLC plates. ^1H, ^{13}C, and COSY nuclear magnetic resonance spectra were recorded on a Bruker AC-300 (300.13 MHz), and Bruker DRX-200 (200.1 MHz) chemical shifts are reported in ppm. Tetramethylsilane was used as an internal standard. IR spectra were obtained using a BIO-RAD Excalibur FTS 3000 FT-IR spectrometer (as KBr pellets). EI mass spectra were recorded using a VG ZAB2F instrument. FAB (Matrix: 3-nitrobenzyl alcohol) mass spectrometry was performed on a JEOL JMS-700 machine. MALDI-TOF mass spectra were recorded on a Bruker Biflex TOF-MS spectrometer in positive reflection mode using Dithranol as matrix. Electrospray ionization mass spectra were recorded on a Finnigan TSQ-700 spectrometer. Absorbance UV/Vis spectra were recorded on a Specord S 100 spectrophotometer (Carl Zeiss Jena). Elemental analyses were performed by the Mikroanalytisches Laboratorium des Organisch-Chemischen Instituts der Universität Heidelberg.

Spectrophotometric Titrations

Titrations yielding mononuclear complexes were performed in pure DMSO at a concentration of 0.5 mM ligand in the presence of 2 equiv. sodium hydroxide. A 2 mM stock solution of $Cu(NO_3)_2{\cdot}3H_2O$, $Ni(NO_3)_2{\cdot}6H_2O$, or $Pd^{II}(CH_3CO_2)_2$ in DMSO was then added in steps of 0.2 equiv. allowing 2 min for equilibration until no further changes in spectra were observed. Final absorptions were corrected for volume changes. Concentrations of the stock solutions used: 1 mM $\mathbf{L}^n$ in DMSO, 0.1 M aqueous NaOH, 2 mm metal salt in DMSO.

Kinetic Studies

Reaction solutions were prepared by combining appropriate amounts of ligand solution (1 mM stock solutions in DMSO), DMSO, $Cu(NO_3)_2{\cdot}3H_2O$ (2 mM stock solution in H_2O), and MOPS-buffer (0.2 M stock solution in H_2O, pH 6.8). The reaction was started by addition of the substrate HPNP (5 mM stock solution in H_2O). For the experiments summarized in Fig. 8, final concentrations in the reaction mixtures were 0.1 mM complex, 0.5 mM HPNP, and 0.02 M MOPS-buffer in water:DMSO 3:1. The concentration of $Cu(NO_3)_2$ varied from 0.3 to 0.8 mM (i.e. 3–8 equiv.; precipitation occurred below this concentration). In experiments with a constant metal concentration, 5 equiv. of Cu^{2+} [0.5 mM $Cu(NO_3)_2$] and 200 equiv. of buffer [0.2 M stock solution of MOPS (pH 6.8, 6.95, and 7.15) or MES (pH 6.5), respectively, in H_2O] were used.

Transesterification of HPNP was followed spectrophotometrically by the release of *p*-nitrophenolate at 400 nm ($\varepsilon = 18{,}600\,M^{-1}\,cm^{-1}$), considering equilibration *p*-nitrophenol/*p*-nitrophenolate at pH 6.8 ($pK_a = 7.15$). The pseudo-first-order rate constants, k_{obs}, were determined from the initial rate of the reaction (<5% conversion). All reported data are average values of at least three measurements (reproducibility ± 15%).

Determination of k_{cat} and K_m by UV–Vis measurements and inhibition experiments were performed in microtitre plates on a Tecan Spectrafluor plus spectrophotometer, and reaction solutions were prepared by a robotic liquid handling system (Genesis 150 workstation, Tecan). MOPS-buffer (0.2 M stock solution in H_2O, pH 6.8), water, and HPNP (varying concentrations from 0.1 mm to 10 mm in H_2O) were added to solutions of the trinuclear complexes $[(\mathbf{L}^n{-}2H)Cu_3]^{4+}$ (0.4 mm stock solution in DMSO using 5 equiv. of copper(II) nitrate; prepared *in situ*). The final concentrations in the reaction mixtures were 0.1 mm complex and 0.02 M MOPS-buffer in water:DMSO 3:1, and the HPNP concentrations varied from 0.2 to 2.5 mm. Reactions were started by addition of the substrate. Transesterification of HPNP was followed spectrophotometrically by the release of *p*-nitrophenolate at 405 nm ($19{,}500\,M^{-1}\,cm^{-1}$), considering equilibration *p*-nitrophenol/*p*-nitrophenolate at pH 6.8 ($pK_a = 7.15$). The pseudo-first-order rate constants, k_{obs}, were determined from the initial rate of the reaction (<5% conversion). All reported data are average values of three measurements (reproducibility ± 15%).

Inhibition experiments were performed in microtitre plates in a similar fashion to the determination of Michaelis–Menten constants. In this case, the HPNP concentration (as 5 mm stock solution in water) was held at 0.5 mm, whereas various inhibiting anion concentrations representing 0.1 up to 50 equiv. (final concentration: 0.01 mm to 5 mm) with respect to the metal complex [prepared from ligand solution 0.5 mm and 5 equiv. $Cu(NO_3)_2$ as 2 mm stock solution] were used. Addition of inhibitor solutions in water was performed shortly before the application of substrate. Appropriate amounts of the following metal salts as stock solutions (100, 20, 10, 5, or 4 mm in water) were used: potassium dihydrogenphosphate, potassium chloride, potassium nitrate, potassium oxalate, potassium perrhenate, sodium actetate, sodium chloride, sodium fluoride, sodium hydrogencarbonate, sodium perchlorate, sodium sulfate, and sodium tetrafluoroborate. The final concentrations in the reaction mixtures were 0.1 mm complex, 0.02 M MOPS-buffer, pH 6.8, 0.5 mm HPNP, and 0.01 mm to 5 mm inhibitor in water:DMSO 3:1.

Ligand Syntheses

1-(2-Pyridyl)-3-methylpropandione-1,3

A mixture of ethyl picolinate (15.1 g, 0.1 mol) and anhydrous acetone (6.97 g, 0.12 mol) was added dropwise to a stirred suspension of sodium ethylate (0.96%, 70.9 g, 0.1 mol) in anhydrous THF (25 mL) at 0°C. Then, the mixture was stirred for 30 min without cooling and then refluxed for 2 h. Glacial acetic acid (7.2 g, 0.12 mol) and water (45 mL) were added after cooling, and THF was distilled off. The residual oil and aqueous layer were extracted with diethylether (4 × 70 mL), combined ether extracts were dried with anhydrous Na_2SO_4, and ether was removed on a rotary evaporator. The oily residue was subjected to vacuum distillation yielding the pure compound (95–97°C, 0.3 torr). Yield: 11.9 g, 73%; ^{1}H-NMR ($CDCl_3$, 200.13 MHz): $\delta = 2.23$ (s, 3H, CH_3), 6.82 (s, 1H, C-H enol), 7.40 (ddd, $J_{3,5} = 1.0$ Hz, $J_{4,5} = 7.7$ Hz, $J_{5,6} = 4.8$ Hz, 1H, Py-5), 7.83 (td, $J_{3,4} = 7.8$ Hz, $J_{4,6} = 1.7$ Hz, 1H, Py-4), 8.07 (d*t*, 1H, Py-3), 8.65 (ddd, Py-6); MS (EI); *m/z* (%): 163.0 (59), 148 (100) $[M\text{-}CH_3]^+$, 78 (80) $[C_5H_4N]^+$; elemental analysis calcd. (%) for $C_9H_9NO_2$ (163.2): C 66.25, H 5.56, N 8.58; found C 66.2 H 5.57, N 8.57.

2-Methyl-6-(2-pyridyl)-pyrimidine

This compound was synthesized by a modified literature method [13]. A mixture of 1-(2-pyridyl)-3-methylpropandione-1,3 (6.8 g, 41.7 mmol) and formamide (75 mL) was gently refluxed for 6 h (the temperature in the oil bath should not exeed 210°C). After cooling, 200 mL of water were added, and then water and formamide were distilled *in vacuo* The distillate was diluted with water (100 mL) and extracted with chloroform (4 × 250 mL). Combined extracts were washed with brine, dried with anhydrous Na_2SO_4, and the solvent distilled off. The crude product was purified by chromatography on silica. The main by-product (forming with a comparable yield) is picolinamide. This remains in the oily residue after distillation of formamide. Yield: 3.0 g, 42%; $R_f = 0.65$ (acetone/hexane 1:10); ^{1}H-NMR ($CDCl_3$, 200.13 MHz): $\delta = 2.62$ (s, 3H, CH_3), 7.39 (ddd, $J_{3,5} = 0.9$ Hz, $J_{4,5} = 7.8$ Hz, $J_{4,5} = 4.8$ Hz, 1H, Py-5), 7.85 (td, $J_{3,4} = 7.8$ Hz, $J_{4,6} = 1.7$ Hz, 1H, Py-4), 8.46 (d, 1H, Py-3), 8.70 (d, Py-6), 9.14 (s, Pym-2)—MS (EI): 171.0 (100) $[M]^+$; elemental analysis calcd. (%) for $C_{10}H_9N_3$ (171.2): C 70.16, H 5.30, N 24.54; found C 70.20 H 5.34, N 24.58.

6-(2-Pyridyl)-pyrimidine-4-carboxylic Acid

Oxidation with SeO_2 was performed analogously to the reported method for 6-phenylpyrimidine-2-carboxylic

acid [43]. A mixture of 2-methyl-6-(2-pyridyl)-pyrimidine (1.0 g, 5.84 mmol) and SeO_2 (1.04 g, 9.37 mmol) was refluxed in pyridine (15 mL) for 6 h. After cooling, the precipitated selenium was filtered off, and the solvent removed. The residue was treated with 1 N aqueous NaOH (8 mL) and washed with CH_2Cl_2 (15 mL). Addition of 1 N HCl (8 mL) to the aqueous layer caused precipitation of off-white material, which was filtered, washed with water, and dried *in vacuo* at 130°C for 3 h. The acid is soluble in methanol, ethanol and hot water and not soluble in hot chloroform. Yield: 1.01 g, 86%; ^{1}H-NMR (d_6-DMSO, 200.13 MHz): $\delta = 7.62$ (ddd, $J_{3,5} = 0.9$ Hz, $J_{4,5} = 7.7$ Hz, $J_{4,5} = 4.8$ Hz, 1H, Py-5), 8.06 (td, $J_{3,4} = 7.7$ Hz, $J_{4,6} = 1.7$ Hz, 1H, Py-4), 8.49 (d, 1H, Py-3), 8.83 (ddd, 1H, Py-6), 8.80 (d, $J_{2,5} = 1.2$ Hz, 1H, Pym-5), 9.45 (s, Pym-2); MS(EI): 201.0 (45) $[M]^+$, 157.0 (100) $[M\text{-}CO_2]^+$; elemental analysis calcd. (%) for $C_{10}H_7N_3O_2$ (201.2): C 59.70, H 3.51, N 20.89; found C 59.53 H 3.55, N 20.95.

N,N′-Bis[4-(2-pyridyl)-pyrimidine-6-carbonyl]-1,3-diaminopropane (L^2)

A suspension of 6-(2-pyridyl)-pyrimidine-4-carboxylic acid (0.2 g, 1 mmol) and 1,1′-carbonyldiimidazol (CDI) (0.18 g, 1.1 mmol) in a mixture of anhydrous THF (20 mL) and DMF (7 mL) was refluxed for 10–15 min until complete dissolution of the solid was achieved. 1,3-Diaminopropane (0.037 g, 0.5 mmol) dissolved in THF (5 mL) was added, and the obtained mixture was refluxed for 12 h. The solvent was removed, and the residue was redissolved in chloroform (30 mL), washed with saturated aqueous NH_4Cl (20 mL), brine, dried with $MgSO_4$, and the solvent distilled off. The crude product was purified by LC on silica (chloroform, then adding up to 2% of methanol to the eluent). Soluble in $CHCl_3$, CH_2Cl_2, acetone, slightly soluble in methanol, toluol, and not soluble in water. Yield: 0.205 g, 93%; $R_f = 0.26$ ($CHCl_3$), 0.42 (CH_2Cl_2/MeOH 97/3); IR (KBr): $\nu = 1675\,cm^{-1}$ (amide(I)-C═O), $3331\,cm^{-1}$ (amide-NH); ^{1}H-NMR ($CDCl_3$, 200.13 MHz): $\delta = 1.97$(m, $^4J = 6.2$ Hz, 2H, β-CH_2), 3.64(q, 4H, α-CH_2), 7.43(ddd, $J_{3,5} = 1.1$ Hz, $J_{4,5} = 7.8$ Hz, $J_{5,6} = 4.8$ Hz, 2H, Py-5), 7.87(td, $J_{3,4} = 7.8$ Hz, $J_{4,6} = 1.1$ Hz, 2H, Py-4), 8.47(tt, 2H, Py-3), 8.52(t, $^3J = 6.2$ Hz, 2H, NH), 8.77(ddd, Py-6), 9.15(d, $J_{2,5} = 1.4$ Hz, 2H, Pym-5), 9.28(d, 2H, Pym-2); ^{13}C-NMR($CDCl_3$, 75.47 MHz): $\delta = 29.82$(β-CH_2), 36.63(α-CH_2), 114.98(Pym-5), 121.84(Py-3), 125.68(Py-5), 137.03(Py-4), 149.87(Py-6), 153.36(Py-2), 157.45, 157.61(Pym-2/6), 163.47(Pym-4), 165.34(C═O); MS(FAB^+): 441.3 (57) $[M + H]^+$, 463.2 (22) $[M + Na]^+$; elemental analysis calcd. (%) for $C_{23}H_{20}N_8O_2$ (440.5): C 62.72, H 4.58, N 25.44; found C 62.80 H 4.63, N 25.38.

N,N′-Bis[4-(2-pyridyl)-pyrimidine-6-carbonyl]-2-aminobenzylamine (L^3)

Synthesis was performed analogously to *N,N′*-bis[4-(2-pyridyl)-pyrimidine-6-carbonyl]-1,3-diaminopropane ($\mathbf{L}^2$) using 6-(2-pyridyl)-pyrimidine-4-carboxylic acid (0.2 g, 1 mmol), CDI (0.18 g, 1.1 mmol), and 2-aminobenzylamine (0.061 g, 0.5 mmol). After 12 h of reflux and cooling, the insoluble residue was filtered and discarded. The solvent was distilled off, and the residue was subjected to extraction with chloroform and LC (similarly to $\mathbf{L}^3$). The product is soluble in $CHCl_3$, CH_2Cl_2, and methanol, and insoluble in water.

Suitable crystals for X-ray analysis were obtained after repeated recrystallization from warm dichloromethane/methanol mixtures and their slow evaporation at room temperature. Yield: 0.066 g, 27%; $R_f = 0.44$ (acetone/hexane 1/9); IR (KBr): $\nu = 1672\,cm^{-1}$ [amide(I)-C═O], $3312\,cm^{-1}$ (amide-NH); ^{1}H-NMR ($CDCl_3$, 200.13 MHz): $\delta = 4.77$ (d, $^3J = 6.1$ Hz, 2H, CH_2), 7.27 (m, 1H, Ph-4), 7.37–7.49 (m, 4H, Py-5 + Ph-3,5), 7.87 (td, $J_{4,5} = 7.8$ Hz, $J_{4,6} = 1.7$ Hz, 2H, Py-4), 8.04 (d, $J_{5,6} = 7.8$ Hz, 1H, Py-6), 8.48 (m, 2H, Py-3), 8.60 (t, 1H, NH aliphat.), 8.78 (ddd, $J_{5,6} = 4.7$ Hz, 2H, Py-6), 9.18 (d, $J_{2,5} = 1.4$ Hz, 1H, Pym-2/5), 9.20 (d, $J_{2,5} = 1.4$ Hz, 1H, Pym-2/5), 9.25 (d, $J_{2,5} = 1.2$ Hz, 1H, Pym′-2/5), 9.31 (d, $J_{2,5} = 1.2$ Hz, Pym′-2/5), 10.60(s, 1H, NH arom.); ^{13}C-NMR ($CDCl_3$, 75.47 MHz): $\delta = 40.75$ (CH_2), 115.05, 115.78, 117.86 (Pym-5, Ph-5, Ph-3), 121.23 (Ph-1), 121.81 (Py-3), 125.73 (Py-5), 129.32 (Ph-4), 130.66 (Ph-6), 137.04 (Py-4), 145.52 (Ph-2), 149.82(Py-6), 153.17(Py-2), 157.06 (Pym-6), 157.45 (Pym-2), 163.13 (Pym-4), 165.38 (C═O); MS (FAB^+): 489.36 (31) $[M + H]^+$, 511.34 (12) $[M + Na]^+$; elemental analysis calcd. (%) for $C_{27}H_{20}N_8O_2$ (488.5): C 66.39, H 4.13, N 22.94; found: C 66.57 H 4.20, N 22.77.

[(L^2–2H)Cu] (1) and [(L^2–2H)Ni] (2)

To $\mathbf{L}^2$ (44 mg, 0.1 mmol) dissolved in the mixture of dichloromethane and methanol (1:4, 10 mL) were added consequently aqueous solution of copper(II) or nickel(II) chloride (1 M, 0.1 mL), respectively, and an aqueous solution of sodium hydroxide (1 M, 0.2 mL) upon continuous stirring at 30–35°C. In the case of the copper system, in 2–3 min, the brown precipitate is formed; in the case of the nickel system, precipitation of orange solid occurs after prolonged heating (ca. 10–15 min) with an increase in temperature up to 50–55°C accompanied by the addition of water in small portions (5 × 1 mL). The precipitates were filtered from the cooled mixtures, washed with water and dried *in vacuo*. The products are virtually insoluble in water and common organic solvents, and

the nickel complex indicates only slight solubility in warm DMSO and DMF.

The crystals of the copper complex used for X-ray analysis were obtained after performing the described synthesis in the solvent mixture where methanol was replaced by DMSO and keeping the obtained solution at room temperature for 72 h.

- **[(L^2−2H)Cu] (1)**: Yield 41 mg, 82%; IR (KBr): $\nu = 1591$ (C═O) cm^{-1}; UV/Vis (DMSO): λ_{max} (ε): 295 (43455), 355 nm (4926) $mol^{-1}\,dm^3\,cm^{-1}$; elemental analysis calcd. (%) for $CuC_{23}H_{18}N_8O_2$ (502.0): C 55.03, H 3.61, N 22.32; found: C 54.76, H 3.60, N 22.04.
- **[(L^2−2H)Ni] (2)**: 43 mg, 86%; IR (KBr): $\nu = 1597$ (C═O) cm^{-1}; elemental analysis calcd. (%) for $NiC_{23}H_{18}N_8O_2$ (497.1): C 55.57, H 3.65, N 22.54; found: C 54.28, H 3.71, N 22.39.

[(L^2−2H)Pd]·H_2O (3)

To $\mathbf{L}^2$ (44 mg, 0.1 mmol) dissolved in the mixture of dichloromethane and methanol (1:4, 10 mL) were added consequently a solution of tetrakis-(acetonotrile)palladium(II) tetrafluoroborate (44 mg, 0.1 mmol) in acetonitrile (3 mL) and an aqueous solution of lithium hydroxide (1 M, 0.2 mL) upon continuous stirring at 30–35°C. In 4–5 min, a yellow precipitate was formed. The solid was filtered from the cooled mixture, washed with methanol and water, and dried *in vacuo*. The product is insoluble in water and common organic solvents and slightly soluble in warm nitrobenzene. Yield: 47 mg, 83%; IR (KBr): $\nu = 1596$ (C═O) cm^{-1}; UV/Vis (DMSO): λ_{max} (ε): 292 (41591), 400 nm (8544) $mol^{-1}\,dm^3\,cm^{-1}$; elemental analysis calcd. (%) for $PdC_{23}H_{20}N_8O_3$ (562.9): C 49.08, H 3.58, N 19.91; found: C 49.07, H 3.44, N 19.65.

[(L^3−2H)Cu]·H_2O·0.5 CH_3OH

This compound was prepared in similar fashion to (**2**) and (**3**) using $\mathbf{L}^3$ (10.1 mg, 0.02 mmol), dichloromethane and methanol (1:4, 6 mL), and aqueous solutions of copper(II) nitrate (1 M, 23 μL) and sodium hydroxide (1 M, 46 μL). The product is soluble in DMSO. Yield 6.4 mg, 55%; IR (KBr): $\nu = 1599$, 1582 (C═O) cm^{-1}; UV/Vis (DMSO): λ_{max} (ε): 298 (43205), 380 nm (5162) $mol^{-1}\,dm^3\,cm^{-1}$; MS(LDI$^+$) m/z = 548.4, 550.4 [calcd. for ($\mathbf{L}^3$−2H)^{63}Cu: 549.1]; MS(ESI$^+$): m/z(%): 550.4 (100) [($\mathbf{L}^3$−2H)^{63}Cu + H]$^+$, 552.4 (54) [($\mathbf{L}^3$−2H)^{65}Cu + H]$^+$; elemental analysis calcd. (%) for $C_{27}H_{20}$-CuN_8O_3 + 0.5CH_3OH: C 56.55, H 3.80, N 19.19; found: C 56.84, H 3.85, N 18.55.

[Cu_{12}(L^2-2H)$_4$(μ_4-C_2O_4)$_2$(μ-OH)$_4$(μ-Cl_4)Cl_4 (H_2O)$_2$]·34.83H_2O (5)

To a stirred solution of $\mathbf{L}^2$ (44.1 mg, 0.1 mmol) in a mixture of dichloromethane and methanol (1:4, 10 mL) at 30°C, consequently aqueous solutions of sodium hydroxide (1 M, 0.2 mL) and copper(II) chloride (1 M, 0.3 mL) were added. The obtained mixture was stirred while gently heating, and after 2 min, an aqueous solution of sodium oxalate (0.1 M, 0.5 mL) was added. The dark green mixture was cooled, the pH was adjusted to 7–8, and the obtained green solution was set for crystallization at room temperature to produce dark green crystals suitable for X-ray analysis within 24–36 h. While drying *in vacuo*, the product loses a part of crystallization water, so that the analytically pure sample contains 11 molecules of solvate water. Yield: 71 mg, 87%; IR (KBr): $\nu = 1610$ (bridging oxalate), 1590 (C═O) cm^{-1}; UV/Vis (H_2O): λ_{max} (ε): 307 (31,648), 318 nm (28,884), 378 nm (3442) $mol^{-1}\,dm^3\,cm^{-1}$; MS(ESI$^+$): $m/z = 1023.5$ (calcd. most abundant isotope peak of $[C_{99}H_{92}Cl_5Cu_{12}N_{32}O_{25}]^{3+}$: 1022.9)); MS(MALDI$^+$) $m/z = 502.1$, 504.1 [($\mathbf{L}^2$−2H)^{63}Cu resp. ^{65}Cu) + H]$^+$, calcd. for [($\mathbf{L}^2$−2H)^{63}Cu + H]$^+$: 502.1; elemental analysis calcd. (%) for $Cu_{12}C_{96}H_{102}N_{32}$-$O_{33}Cl_8$ (3278.2): C 35.17, H 3.14, N 13.67; found: C 35.13, H 3.17, N 13.57.

X-ray Crystallography

Details of the X-ray data collection and refinement are given in Table III.[†] Intensities were measured using a Bruker AXS Smart 1000 diffractometer at 190 K. Corrections for Lorentz and polarization effects were applied. Absorption corrections were performed by a semi-empirical method based on multiple scans of equivalent reflections using the SADABS routine [44]. The structure was solved by direct methods and refined by full-matrix, least-squares on all F_o^2 using SHELXTL NT V.5.1 [45]. The non-hydrogen atoms were refined anisotropically. The positions of aromatic and methylene protons in all the structures were set on calculated positions, and the protons of the bridging OH-groups in [Cu_{12}($\mathbf{L}^2$−2H)$_4$(μ_4-C_2O_4)$_2$(μ-OH)$_4$-(μ-Cl_4)Cl_4(H_2-O)$_2$]·34.83H_2O (**5**) were located from

[†]Crystallographic data (excluding structure factors) for the structure included in this paper have been deposited with the Cambridge Crystallographic Crystallographic Data Centre as supplementary publication no. CCDC-129330 ($\mathbf{L}^3$), CCDC-192329 (**5**), CCDC-192328 (**1**). Copies of the data can be obtained free of charge on application to CCDC, 12 Union Road, Cambridge CB2 1EZ, UK. Fax: +44-1223-336-033; E-mail: deposit@ccdc.cam.ac.uk.

TABLE III Crystal data and structure refinement for $\mathbf{L}^3$, **1**, **5**

Compound	$\mathbf{L}^3$	**1**	**5**
Empirical formula	$C_{27}H_{20}N_8O_2$	$C_{23}H_{18}N_8O_2Cu$	$C_{96}H_{149.66}N_{32}O_{56.83}Cl_8Cu_{12}$
M	488.51	502.00	3707.50
Wavelength	0.71073 Å	0.71073 Å	0.71073 Å
Crystal system	Monoclinic	Monoclinic	Monoclinic
Space group	$P2(1)/c$	$C2/c$	$C2/c$
a/Å	6.7791(13)	20.4050(17)	48.956(2)
b/Å	21.724(4)	9.4480(7)	20.7509(9)
c/Å	15.535(3)	10.6408(8)	36.1738(16)
β/°	92.863(5)	98.592(2)	130.6600(10)
U/Å^3	2284.9(8)	2028.4(3)	27877(2)
Z	4	4	8
ρ_{calcd}/Mg m^{-3}	1.420	1.644	1.767
ν/mm^{-1}	0.095	1.120	2.045
$F(000)$	1016	1028	15106
Crystal size/mm	0.41 × 0.10 × 0.01	0.24 × 0.21 × 0.15	0.30 × 0.24 × 0.15
θ range/°	1.87–25.00	2.38–30.51	1.10–28.24
Range hkl	−8–8,0–25,0–28	−29–28,0–13,0–15	−61–49, 0–27, 0–48
Reflections collected	13510	9058	96393
Independent reflections	4008	3092	32726
Reflections with $I > 2\sigma(I)$	2543	2413	23485
Data/parameters	4008/414	3092/200	32726/1951
Goodness-of-fit on F^2	1.020	1.079	1.059
Final R indices [$I > 2\sigma(I)$]	$R1 = 0.0460, wR2 = 0.0998^{*,\dagger}$	$R1 = 0.0361, wR2 = 0.0813^{*,\dagger}$	$R1 = 0.0465, wR2 = 0.1261^{*,\dagger}$
Final R indices (all data)	$R1 = 0.0882, wR2 = 0.1181^{*,\dagger}$	$R1 = 0.0555, wR2 = 0.0927^{*,\dagger}$	$R1 = 0.0759, wR2 = 0.1467^{*,\dagger}$

$^{*}R1 = \Sigma(F_o - F_c)/\Sigma F_o$. †wR2 = $\{(w(F_o^2 - F_c^2)^2]/([w(F_o^2)^2]\}^{1/2}$.

a difference Fourier map and included in refinement. In the **5** structure, only part of the water molecule protons was observed on difference Fourier maps, and their positional and isotropic thermal parameters were fixed during the further stages of refinement. Additionally, several solvate water molecules were found to be disordered between two positions or to have occupancy factors less than 1. In the structure of [($\mathbf{L}^2$–2H)Cu] (**1**), the propylene carbons [C(34), C(1), and C(34A)] were found to be disordered between two positions with equal occupancy.

Acknowledgements

This work was funded by the Deutsche Forschungsgemeinschaft (Gerhard Hess-Programm) and supported by the Fonds der Chemischen Industrie.

References

[1] Krämer, R.; Gajda, T. In *Perspectives on Bioinorganic Chemistry*; Hay, R. W., Dilworth, J. R., Nolan, K. B., Eds.; JAI Press, Greenwich, 1999; Vol. 4, pp 209–240.
[2] Williams, N. H.; Takasaki, B.; Chin, J. *Acc. Chem. Res.* **1999**, *32*, 485.
[3] Molenveld, P.; Engbersen, J. F. J.; Reinhoudt, D. N. *Chem. Soc. Rev.* **2000**, *29*, 75.
[4] Kühn, U.; Warzeska, S.; Pritzkow, H.; Krämer, R. *J. Am. Chem. Soc.* **2001**, *123*, 8125–8126.
[5] Ahlers, B.; Cammann, K.; Warzeska, S.; Krämer, R. *Angew. Chem.* **1996**, *108*, 2270.
[6] Chapman, Jr, W. H.; Breslow, R. *J. Am. Chem. Soc.* **1995**, *117*, 5462.
[7] Meyer, F.; Kaifer, E.; Kircher, P.; Heinze, K.; Pritzkow, H. *Chem. Eur. J.* **1999**, *5*, 1617.
[8] Fritsky, I. O.; Ott, R.; Krämer, R. *Angew. Chem., Int. Ed.* **2000**, *39*, 3255–3258.
[9] Fritsky, I. O.; Ott, R.; Pritzkow, H.; Krämer, R. *Chem. Eur. J.* **2001**, *7*, 1221–1231.
[10] Scarso, A.; Scheffer, U.; Göbel, M.; Broxterman, Q. B.; Kaptein, B.; Formaggio, F.; Toniolo, C.; Scrimin, P. *Proc. Natl Acad. Sci. USA* **2002**, *99*, 5144–5149.
[11] Kirby, A. J. *Angew. Chem. Int. Ed.* **1996**, *35*, 706–722.
[12] Molenveld, P.; Engbersen, J. F. J.; Kooijman, H.; Spek, A. L.; Reinhoudt, D. N. *J. Am. Chem. Soc.* **1998**, *120*, 6726–6737.
[13] Lafferty, J. J.; Case, F. H. *J. Org. Chem.* **1967**, *32*(5), 1591–1596.
[14] Peisach, J.; Blumberg, W. E. *Arch. Biochem. Biophys.* **1974**, *165*, 691.
[15] Tamura, M.; Kajikawa, Y.; Azuma, N.; Tani, H.; Tajima, K.; Kanaori, K.; Makino, K.; Takayama, T. *Acta Crystallogr.* **1999**, *C55*, 719–722.
[16] Stephens, F. S.; Vagg, R. S. *Inorg. Chim. Acta* **1984**, *88*, 7–14.
[17] Tsuboyama, S.; Sakurai, T.; Kobayashi, K.; Azuma, N.; Kajikawa, Y.; Ishizu, K. *Acta Crystallogr.* **1984**, *B40*, 466–473.
[18] Stephens, F. S.; Vagg, R. S. *Inorg. Chim. Acta* **1982**, *57*, 43–49.
[19] Warzeska, S.; Krämer, R. *Chem. Ber.* **1995**, *128*, 115–119.
[20] Nonoyama, K.; Ojima, H.; Ohki, K.; Nonoyama, M. *Inorg. Chim. Acta* **1980**, *41*, 155.
[21] Curtis, N. F. *J. Chem. Soc., A* **1968**, 1584.
[22] Shibahara, T.; Ooi, S.; Kuroya, H. *Bull. Chem. Soc. Jpn.* **1982**, *55*, 3742.
[23] Cotton, F. A.; Chun Lin, C. A. *J. Chem. Soc., Dalton Trans.* **1998**, 3151.
[24] Cotton, F. A.; Daniels, L. M.; Chun Lin; Murillo, C. A. *J. Am. Chem. Soc.* **1999**, *121*, 4538.
[25] Johnson, B. F. G.; Lewis, J.; Raithby, P. R.; Saharan, V. P.; Wing, Tak Wong; *Chem. Commun.* **1991**, 365.
[26] Deal, K.; Burstyn, J. N. *Inorg. Chem.* **1996**, *35*, 2792–2798.
[27] Liang, G.; Tribolet, R.; Sigel, H. *Inorg. Chem.* **1988**, *27*, 2877.
[28] Morrow, J. R.; Trogler, W. C. *Inorg. Chem.* **1988**, *27*, 3387–3394.
[29] Bailey, N.; Carrington, A.; Lott, K.; Symons, M. *J. Chem. Soc.* **1960**, 290.
[30] Fabrizzi, L.; Pallavicini, P.; Parodi, L.; Taglietti, A. *Coord. Inorg. Chim. Acta* **1993**, *238*, 5–8.
[31] Amendola, V.; Fabrizzi, L.; Mangano, C.; Pallavicini, P.; Poggi, A.; Taglietti, A. *Coord. Chem. Rev.* **2001**, 219–221, 821–837.
[32] Banerjea, D.; Kaden, T.; Sigel, H. *Inorg. Chem.* **1981**, *20*, 2586.

[33] Zhao, J.; Song, B.; Saha, N.; Saha, A. *Inorg. Chim. Acta* **1996**, *250*, 185 (extrapolated value for ion strength $\mu = 0.01$ M).
[34] McAuley, A.; Nancollas, G. *Trans. Farad. Soc.* **1960**, *56*, 1165.
[35] Zuehelke, R.; Kester, D. *Marine Chem.* **1983**, *13*, 203. The value at $\mu = 0.01$ M was obtained by extrapolation, using the dependence on ion strength of the Cu^{2+} binding constant *K* of acetate.
[36] Hemmes, P.; Petruci, S. *J. Phys. Chem.* **1970**, *74*, 467.
[37] Gifford, S.; Cherry, W. *Inorg. Chem.* **1974**, *13*, 1434.
[38] Yamaguchi, K.; Akagi, F.; Fujinami, S.; Suzuki, M.; Shionoya, M.; Suzuki, S. *Chem. Commun.* **2001**, 375–376.
[39] Wall, M.; Hynes, R. C.; Chin, J. *Angew. Chem., Int. Ed. Engl.* **1993**, *32*, 1633.
[40] Uchimaru, T.; Tsuzuki, S.; Storer, J. W.; Tanabe, K.; Taira, K. *J. Org. Chem.* **1994**, *59*, 1835–1843.
[41] Uchimaru, T.; Uebayasi, M.; Tanabe, K.; Taira, K. *FASEB J.* **1993**, *7*, 137–142.
[42] Brown, D. M.; Usher, D. A. *J. Chem. Soc.* **1965**, 6558.
[43] Sakamoto, T.; Sakasai, T.; Yamanaka, H. *Chem. Pharm. Bull.* **1980**, *28*(2), 571–577.
[44] Sheldrick, G. M. *SADABS, Program for Scaling and Correction of Area Detector Data*; University of Göttingen: Göttingen, Germany, 1996.
[45] Sheldrick, G. M. *SHELXTL NT V.5.1, Bruker AXS, Program for Crystal Structure Solution and Refinement*; Madison, WI, 1998.